# Pressure Sensors and Filtering Techniques for Stone Stability Assessment

Bas Hofland
report no. 4-01

July 2001

Report submitted to:
Ministry of Transport, Public Works and Water Management
Road and Hydraulic Engineering Division
Contract no. DWW-1700
and
Delft Cluster
Theme: Coast and river
Project: Behaviour of Granular Structures

TU Delft
Technische Universiteit Delft

**Faculteit Civiele Techniek en Geowetenschappen**

# Pressure Sensors and Filtering Techniques for Stone Stability Assessment

Bas Hofland
report no. 4-01

July 2001

Report submitted to:
Ministry of Transport, Public Works and Water Management
Road and Hydraulic Engineering Division
Contract no. DWW–1700
and
Delft Cluster
Theme: Coast and river
Project: Behaviour of Granular Structures



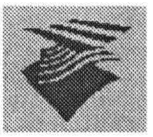

Fluid Mechanics Section, Faculty of Civil Engineering and Geosciences, Delft University of Technology, P.O. Box 5048, 2600 GA, The Netherlands. Tel. +31 15 27 84069; Fax +31 15 27 85975; E-mail: b.hofland@citg.tudelft.nl

# Contents


**1 Introduction** **3**

**2 Wall pressures and stone stability** **5**
2.1 Introduction . . . . . 5
2.2 Pressure integration model . . . . . 6

**3 Research on wall pressures** **9**
3.1 Introduction . . . . . 9
3.2 Key features . . . . . 10

**4 Pressure sensors** **13**
4.1 Introduction . . . . . 13
4.2 Requirements of the pressure sensor . . . . . 13
4.3 The search . . . . . 15
4.3.1 Druck . . . . . 15
4.3.2 Honeywell . . . . . 16

**5 Noise sources** **17**
5.1 Introduction . . . . . 17
5.2 Possible sources . . . . . 18

**6 Filtering Techniques** **20**
6.1 High pass filtering . . . . . 20
6.2 Difference method . . . . . 20
6.3 The 'optimal filter' . . . . . 22

**7 Experimental set-up** **26**
7.1 Flow conditions . . . . . 26
7.1.1 Experiments . . . . . 26
7.1.2 Data processing . . . . . 27
7.2 Stagnant water . . . . . 28
7.3 Simultaneous vibration and pressure measurements . . . . . 28

**8 Results** 29
8.1 Short waves . . . 29
8.2 Long waves . . . 31
8.3 Natural frequencies of flume . . . 31
8.4 Vibrations due to pumps . . . 33
8.5 Electromagnetic disturbance . . . 33
8.6 Turbulence wall pressures . . . 33
8.7 Sensor characteristics . . . 37
8.7.1 Frequency effects . . . 37
8.7.2 Spatial resolution . . . 37
8.8 Temperature dependence . . . 38
8.9 Background noise . . . 39
8.9.1 General . . . 39
8.9.2 Discretisation . . . 39
8.10 Long term stability . . . 39
8.11 Reference pressure . . . 40

**9 Conclusions** 41

**References** 43

**A Companies contacted** 45

**B Technical specifications of *Druck* sensor** 46

**C Technical specifications of *Honeywell* sensor** 47

**D Definitions of spectral functions** 48

# Chapter 1

# Introduction

This report is part of a Ph.D. research project regarding the stability of stones in the top layer of a granular filter. A literature survey (Hofland, 2000) showed that there is still a lack of knowledge of the link between the (turbulence) velocity fluctuations in the flow above a granular filter and the fluctuating forces that act on the stones in the filter. This knowledge is of importance for the design of the granular filters that are part of many hydraulic structures. Therefore experiments are planned in order to get a better insight into the flow characteristics that determine the initiation of motion of the stones, and especially into the influence of the turbulence structure. This will be done on micro scale (i.e. spatial dimensions of a few stone diameters) in order to capture velocity and pressure fluctuations at and near a single stone (or roughness element). For these measurements miniature pressure sensors are required, besides the 'standard' velocity measurement techniques like LDA and PIV. These sensors were not available at the Fluid Mechanics Laboratory, so the acquisition of the pressure sensors and the development of the accompanying signal processing techniques are additional goals that are vital to the measurements. The measurements of the low-magnitude pressure fluctuations are very sensitive to several kinds of noise. So the different sources of noise, and techniques that can be used to prevent or eliminate them are a main focus of the report.

This report is structured as follows: In chapter 2 the importance of wall pressures with respect to the present research is described. The literature on wall pressures that was used, and some general features of wall pressure fluctuations are subsequently described in chapter 3. Chapter 4 deals with the pressure sensors. It begins with a brief description of some general features of pressure sensors. Then the criteria for the required pressure sensor are given. This is followed by a description of the two types of pressure sensors, which were acquired from commercial companies.

The character of the noise that is present in the measured pressure signal is described in chapter 5. This chapter ends with a list that comprises numerous possible sources of noise. A few dedicated filtering techniques that can be used to attenuate the vibrational and acoustical noise are described in the next chapter (chapter 6).

Several experiments were executed in order to get a further idea of the possibilities of the sensors, and the nature of the noise that will be present in the measured signal. The set-up of these experiments is described in chapter 7. An analysis of the tests that were executed is given in chapter 8. In this chapter the nature and magnitude of the various sources of noise are described.

Chapter 9 presents the conclusions of the report. Based on these conclusions the requirements

for the experimental facilities that are needed for the final experiments, and the choice of the best suited pressure sensor are given.

The Ph.D. research is conducted by Bas Hofland at the Fluid Mechanics Laboratory at the Faculty of Civil Engineering and Geosciences of Delft University of Technology. The research is funded by the Road and Hydraulic Engineering Division of the Ministry of Transport, Public Works and Water Management and is co-funded by Delft Cluster, where it is part of the theme 'Coast and River', under the cluster project 'Behaviour of Granular Structures'.

# Chapter 2

# Wall pressures and stone stability

## 2.1 Introduction

Wall pressure fluctuations are of importance to stone stability. They either have a direct influence on stone stability, or can be used to indicate the magnitude of the destabilizing forces (flow and turbulence) that act on a stone protection layer. For example, this is indicated by the fact that behind a backward-facing step both the maximum levels of pressure fluctuations and the maximum entrainment of stones are present at the same position, i.e. a few step heights behind the re-attachment point (De Gunst, 1999; Lauchle & Kargus IV, 1999; Xingkui & Fontijn, 1993). The present generation of pressure sensors makes it possible to investigate this process on a micro scale. As a lot of research has been done on wall pressures at hydraulically smooth walls, we can compare the wall pressure measurements that are to be carried out in this project to results in the literature, and consequently check the performance of the pressure sensors.

Uittenbogaard *et al.* (1998) developed a model, with which a rough estimation can be made of the magnitude of the wall pressures, from the output of a k-$\epsilon$ CFD model. For the subsequent determination of the forces on the stones and the entrainment –using the pressure fluctuations and the friction velocity– a very crude approximation is used. The (Fourier) components of the pressure with wave lengths longer than the stone diameter are incorporated with a constant weighting factor, and the rest of the components is discarded.

Turbulence eddies of different spatial and temporal scales will interact differently with the stones. Booij (1998) estimates that eddies with a size comparable to that of the stone will give the most effective pressure gradient for creating forces on a stone. But this does not mean that eddies with other length scales and a large energy content cannot have a significant influence on stone stability. Therefore a proper weighting factor has to be incorporated in a model.

An indication of the possible effect of the turbulence wall pressures on the stone stability can be obtained from determining a transfer function between the (power) spectrum of the wall pressures and the (power) spectrum of the forces on a stone located in that pressure field. This approach is demonstrated in the following section. It is a first attempt to check the relevance of pressure fluctuations for the determination of stone stability.

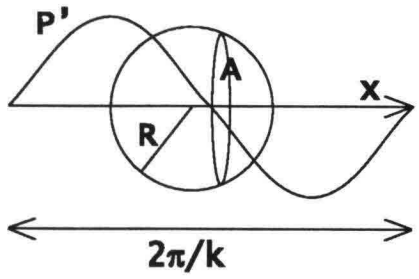


Figure 2.1: Definitions

## 2.2 Pressure integration model

The model regards a stone in a stationary wall flow. The mean forces are not taken into account. Only the effect of a convecting, 'frozen' pressure field is determined. The assumptions are made that the pressure only varies in the flow direction, and that the pressure is not changed by the stone. The stone is schematised as a sphere, see figure 2.1. The assumptions are:

$$\begin{aligned} F'_D(k,\theta) &= \textstyle\int_{-R}^{R} p'(x,k,\theta)\frac{dA}{dx}dx \\ p'(x,k,\theta) &= \hat{p}(k)sin(kx+\theta) \\ A(x) &= \pi(R^2-x^2) \end{aligned} \tag{2.1}$$

$F'_D(k,\theta)$ is the drag force caused by the (Fourier) component of the fluctuating pressure, $p'(x,k,\theta)$, with wave number $k$ and phase $\theta$, $R$ is the radius of the stone, $x$ is the longitudinal coordinate, and $A(x)$ is the cross-sectional area of the stone.

After substitution and solving the integral in eq. 2.1, the force becomes:

$$F'_D(k,\theta) = 4\pi R^2\hat{p}(k)\left(\frac{cos(kR)}{kR} - \frac{sin(kR)}{(kR)^2}\right)cos(\theta) \tag{2.2}$$

This is the transfer function between $p'$ and $F'$. In order to obtain some estimates of average values, we average $F'^2_D$ over all possible phases, divide the equation by $\overline{p'^2(k)} = \frac{1}{2}\hat{p}^2(k)$, and take the square root. This gives the gain factor, $|H_{p,F_D}(k)|$, from the pressure spectrum to the force spectrum. It can be denoted as:

$$|H_{p,F_D}(k)| = 4\pi R^2\left|\frac{cos(kR)}{kR} - \frac{sin(kR)}{(kR)^2}\right| \tag{2.3}$$

So, when a known wall pressure spectrum is taken as a starting point, an estimate of the magnitude of the influence of the wall pressures on the drag force can be made. This force can be used as an indication of the (in-) stability of the stones.

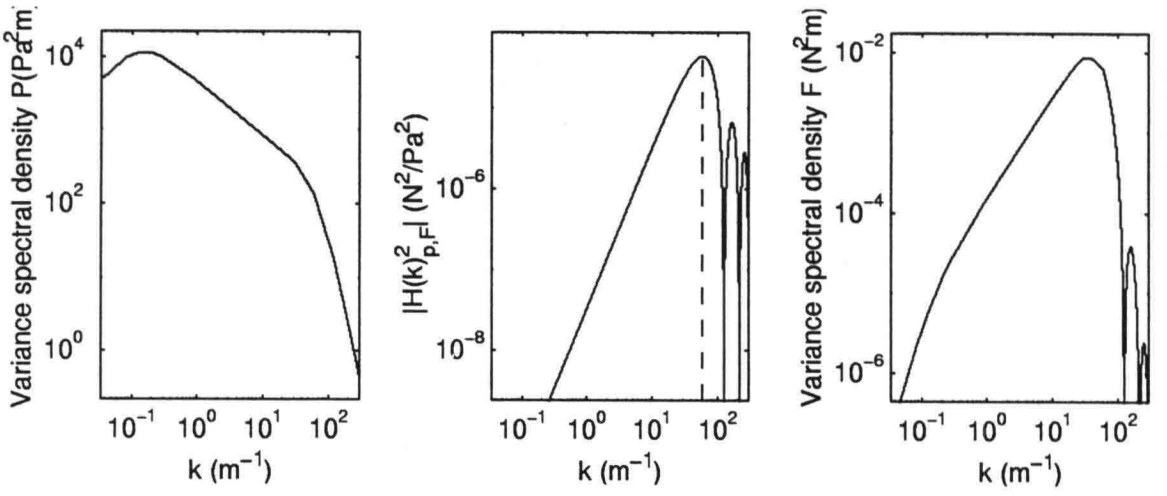


Figure 2.2: Autospectrum of pressures on rough bed (left), Gain factor squared (middle), and autospectrum of estimated forces

**Example**

Now we will examine whether wall pressures possibly influence stone stability directly in a prototype situation. A uniform open channel flow without increased turbulence intensity is chosen for this. The spectra in figure 2.2 show the wall pressures under the uniform current and how the pressure spectrum is transformed into a spectrum of forces on a stone by eq. (2.3). The flow parameters are: depth-averaged flow velocity ($\bar{u}$) is 2 m/s, water depth is 0.5 m, and the Shields parameter is 0.04, from which it follows that the stone diameter ($d$) is 7 cm.

The wall pressures (left plot of fig. 2.2) are obtained from Blake (1970) who measured wall pressures at a rough bed in a wind tunnel. The wall pressures for the wind tunnel flow are scaled to represent the flow parameters for the present case. Although an open channel flow has different turbulence characteristics than a zero pressure gradient channel flow, the pressure fluctuation characteristics for the mid and high frequency ranges –which scale with stone diameter and friction velocity– are expected to be similar, as they are generated by near bed flow processes (see section 8.6), and the influence of a free surface on these is insignificant. For the low frequencies however, they are expected to differ, but they are used as no other information is available. For the transformation of the spectrum from $\omega$ to $k$, the relation $k = \omega/u_c$ is used. Here $u_c$ is the convection velocity of the pressure field, for which the value $u_c = \frac{1}{2}\bar{u}$ is taken.

The middle and right plots show the gain factor, and the estimated force spectrum respectively, obtained from $G_{F_D F_D} = |H_{p,F_D}(k)|^2 G_{pp}$, where $G_{ii}$ is the auto spectrum of a signal $i$.

The graphs in figure 2.2 demonstrate that especially the pressure fluctuations with wavelengths of the same order of magnitude as the diameter of the stone ($\lambda = 2\pi/k \approx 1.5\ d$, see dotted line in fig. 2.2) contribute to the forces on the stones and will hence be important for the determination of the stability of the stones. This agrees with the notion of Booij (1998), who reasoned that fluctuations with twice the size of a stone would create the most effective pressure gradient.

When the power spectrum of the drag force is integrated, an estimation of the variance of

the wall-pressure-induced drag force variations is obtained. In the present example three times the standard deviation of the drag force (an often used value for the "maximum" pressure) is equal to about 70% of the gravitational force on a stone. This means that the extreme values of the fluctuating forces calculated by the model are of the same order of magnitude as the average forces on the stone. Therefore it is likely that the forces that are directly generated by turbulence pressure fluctuations play a role and must be taken into account when regarding stone stability. Direct measurements of the forces on a stone, showed larger fluctuating drag forces, see for instance Xingkui & Fontijn (1993), so other mechanisms are also expected to increase the drag force.

**Concluding remarks**

The model still is highly idealised. For instance, at the moment only drag-forces are calculated, although the same approach is possible for the lift force. Furthermore, the model only is a zero-order approach, i.e. the effect of the stone on the pressure field is not taken into account. Experiments must show to which extent this is a valid assumption. Moreover, pressure gradients with lower frequencies or wave numbers can create larger forces in another way which is not taken into account. These large-scale fluctuations can generate large scale velocity fluctuations which might create quasi-steady drag and lift forces.

If the model is to be used for the determination of the entrainment of stones, more effects are of importance. First of all the duration of the forces is of importance. From Newton's second law it directly follows that the force needed to displace a certain mass (stone) along a certain distance in time $T$, is proportional to $T^{-2}$ (this is true when the difference between the resisting force and average force is small compared to the amplitude of the fluctuating force). This means that the force needed to displace a stone is proportional to $\omega^2$, which would indicate an influence on the entrainment rate of $\omega^{-2}$. Furthermore the wave lengths obtained from a spectrum ($\lambda = 2\pi/k$) are not necessarily equal to the size of an eddy, which can be made up of several components. Therefore the representation with a variance density spectrum does not necessarily give a complete physical description of the phenomenon. The phase lag might not be random, which would imply that extreme forces might not be given as a function of the standard deviation of the force only.

Although the model presented above is not perfect, it indicates that the pressure fluctuations could give a significant contribution to the stability of stones. For now, this was only shown for a uniform flow, but for flow configurations with an increased turbulence intensity, the relative contribution of the fluctuating forces compared to the average forces is expected to increase. The model also shows that the length scale of the turbulence fluctuations relative to the stone diameter is of influence, and that this must be incorporated in stability models.

# Chapter 3

# Research on wall pressures

## 3.1 Introduction

A literature survey on wall-pressure research was undertaken. The literature in this field is mainly aimed at other fields of application, like naval and acoustical applications; yet a lot of aspects –like pressure scaling laws, measuring equipment used, and data-processing techniques– are of interest to the present research. Unfortunately, rough boundaries have hardly been studied. A brief overview of the most important research is given below. The key features from this research are given in section 3.2.

Blake (1970) measured the turbulence wall pressures under a developing boundary layer on both smooth and rough walls. The scaling and shape of the spectrum appeared to be similar for both walls, with the distinction that the length scale that can be used to collapse the high-frequency part of the spectrum is the roughness height for the rough wall, and the viscous length scale ($\nu/u_*$) for the smooth wall. Also the influence of various spatial densities of roughness-elements was investigated.

Schewe (1983) measured wall pressures in a wind tunnel, and determined conditional averages of the extreme pressure fluctuations with amplitudes larger than 4 times the standard deviation. The dimensionless diameter of the (pinhole above the) pressure sensor ($d^+ = du_*/\nu = 19$) appeared to be small enough to capture all turbulence length scales .

Blake (1986) wrote a book on flow induced sound and vibrations. This is an elaborate and good reference book.

Farabee & Casarella (1991) did very precise measurements on wall pressures in a wind tunnel. These measurements are possibly the best so far, and give a good overview of the various types of scaling of turbulence wall pressures.

Löfdahl *et al.* (1993) made a very small pressure sensor ($d = 1$ mm, $d^+ = 30 - 70$), using microchip technology, and were able to measure very small turbulence scales directly, instead of using a pinhole. In later research the size was reduced further.

Naguib *et al.* (1996) mention a filtering technique for pressure measurements with which it is possible to extract the time records, which had not been used before. See section 6.3 for a further description.

Gravante *et al.* (1998) did detailed measurements of wall pressures in a wind tunnel, confirming many previous results. Their small pressure sensors could capture a large frequency range, and dependence of the r.m.s. of the pressure fluctuations on the Reynolds number effect could be determined.

Chang *et al.* (1999) proved, with the aid of a DNS-calculation, that the turbulence term in the Poisson equation cannot be neglected in comparison to the mean shear term, when the turbulence wall pressures (TWP) are being calculated, although the opposite was expected until then. In most TWP models, these terms were neglected.

Lauchle & Kargus IV (1999) found a scaling law for wall pressures behind a backward-facing step. This can be helpful when this kind of flow will be examined in the present research.

## 3.2 Key features

Wall pressure fluctuations in an incompressible fluid are described by the Poisson equation for pressure fluctuations:

$$\nabla^2 p = -\rho \frac{\partial^2 (U_j u_i + U_i u_j + u_i u_j - \overline{u_i u_j})}{\partial x_i \partial x_j} \tag{3.1}$$

where $U$ is the time averaged velocity, $u$ is the instantaneous deviation of $U$, $\rho$ is the specific mass density of water, $i, j = x, y, z$, and $p$ is the instantaneous pressure fluctuation.

This is an elliptic equation, so the pressures are dependent on all the sources in the domain. For a 2D shear flow, where the mean flow is in the $x$-direction and only varies in $z$-direction, this can be denoted as:

$$\nabla^2 p = -2\rho \frac{\partial U}{\partial z}\frac{\partial w}{\partial x} - \rho \frac{\partial u_i}{\partial x_j}\frac{\partial u_j}{\partial x_i} + \rho \frac{\partial^2}{\partial x_i \partial x_j}\overline{u_i u_j} \tag{3.2}$$

The first term in eq. 3.2 is the so called mean-shear term. Chang *et al.* (1999) derived from a DNS calculation of a fully developed turbulent channel flow that this term is responsible for a little over 50% of the pressure fluctuations. Most models that are used for the determination of the velocity sources of the pressure fluctuations are based on this term. Whether this is possible without taking into account the other (turbulence) terms is rather questionable, although the profile of the magnitude of the source terms over the depth is similar.

#### Root-mean-square value

The exact value of the standard deviation of the TWP under a developing boundary layer flow is hard to determine, as the frequency band of pressure fluctuations that contribute to the total variance is very wide. Farabee & Casarella (1991) give an approximation of the value as a function of the Reynolds number, which they obtained from integrating the pressure spectra that were based on their measurements and scaling laws.

$$\begin{aligned} u_*\delta/\nu < 333 &\Rightarrow \frac{\overline{p^2}}{\tau_w^2} = 6.5 \\ u_*\delta/\nu \geq 333 &\Rightarrow \frac{\overline{p^2}}{\tau_w^2} = 6.5 + 1.86\ln(\tfrac{u_*\delta}{\nu 333}) \end{aligned} \tag{3.3}$$

| Frequency range | Outer variable scaling | Inner variable scaling | 4 |
|---|---|---|---|
| Low | $\omega\delta/u_* \leq 5$ | none | ? |
| Mid | $5 < \omega\delta/u_* \leq 100$ | $\omega\nu/u_*^2 \leq 100/\frac{u_*\delta}{\nu}$ | ? |
| Overlap | $100 < \omega\delta/u_* \leq 0.30\frac{u_*\delta}{\nu}$ | $100/\frac{u_*\delta}{\nu} < \omega\nu/u_*^2 \leq 0.30$ | ? |
| High | $0.30\frac{u_*\delta}{\nu} < \omega\delta/u_*$ | $0.30 \leq \omega\nu/u_*^2$ | ? |

Table 3.1: Spectral regions according to Farabee & Casarella (1991)

where $\delta$ is the boundary layer height, $u_*$ is the shear velocity, $\nu$ is the kinematic viscosity, and $\tau_w$ is the bed shear stress.

### Spectral shape

A number of power-laws have been predicted for the power spectrum of the TWP under a developing boundary layer flow by various authors. These power laws are also measured (Gravante *et al.*, 1998; Farabee & Casarella, 1991). In the low frequency range (see table 3.1 for the definition of regions), the variance density increases with the frequency to the power 2. In the mid region a maximum is present at $\omega\delta/u_* \approx 50$. The scaling variables used most frequently in the low and mid frequency range are $\delta$ and $u_*$, although other variables are possible. Farabee & Casarella (1991) state that the scaling behaviour in the low-frequency range will be different in channel flow, as these pressures are probably determined by the rotational flow outside the developing boundary layer.

The scaling variables used for the high frequency range are $\nu$ and $u_*$, which are related to the viscous sub layer. A frequency range exists (overlap range) where the spectrum scales on both inner and outer variables. Here it decreases by $\omega^{-1}$. The velocity sources of these pressures are thought to be situated in the log-region of the boundary layer. The width of this range increases with increasing Reynolds number (table 3.1). In the high frequency range, a power law according to $\omega^{-7/3}$ is predicted, but it has not clearly been measured. For the highest frequencies, the pressures fall off according to the power law $\omega^{-5}$.

### Rough boundaries

The wall pressures under a rough boundary layer flow show the same scaling behaviour for the low frequencies. The high-frequency pressures collapse when the roughness height is used as the characteristic length scale. The dimensionless frequency and spectral density, which collapse on higher frequencies are now: $\omega^+ = \omega\bar{k}_g/u_*$ and $G_{pp}^+(\omega^+) = G_{pp}(\omega)u_*/\tau_w^2\bar{k}_g$, where $\bar{k}_g$ is the arithmetic mean roughness diameter. The spacing between the roughness elements is of influence to a lesser extent than the height (Blake, 1970). The r.m.s.-value of the pressure fluctuations (scaled by the dynamic pressure) is roughly equal to that on smooth walls.

### Extreme pressures

Pressure fluctuations with a value of 4 times the standard deviation of the TWP have been found. Correlation of pressures with velocities did give clear origins for positive pressures. They can be seen to be located near shear layers with a velocity deficit, followed by fast moving flow. For the negative pressures, no clear velocity sources have been found, however. All these results were obtained with smooth walls.

### Applications

An application of wall pressure measurements similar to that at issue is given by Armenio *et al.* (2000). In their paper the r.m.s. pressure fluctuations behind a combined hydraulic jump and backward-facing step are measured as a function of downstream position. These are used for the stability of concrete slabs in spillway stilling basins. The maximum levels of the pressure fluctuations downstream of the step were 6 to 14 times the dynamic pressure of the inflow ($\frac{1}{2}\rho u^2$), except for the case where the main flow was deflected to the upper layer of the flow, where the fluctuations were only 2 times the dynamic pressure of the inflow.

# Chapter 4

# Pressure sensors

## 4.1 Introduction

Most techniques for measuring pressure are based on measuring the movement of a diaphragm that divides two mediums. The first medium is subject to the (varying) pressure that is to be measured and the second medium has a known (reference) pressure. The way the displacement is measured can vary. In the past it was done mechanically; these sensors were large, could not measure high frequencies and were also not very accurate. More modern techniques that are being used for commercial purposes are capacitance and piezo-resistive methods. The first of these methods has a decreasing accuracy with decreasing sensor size, the second is sensitive to changes in temperature. Custom-made pressure sensors of the piezo-resistive type have already been used for measuring turbulent pressure fluctuations in wind tunnels (Löfdahl *et al.*, 1993, for example). Also microphones with a small pinhole, that decreases the sensor diameter, are used. The reference pressure can be one of three main types: absolute, gauge, or differential. When the reference pressure is nearly a vacuum, it is called an absolute type of sensor. When it is connected to the atmosphere, it is called a gauge, and when it is connected to a varying pressure, that has to be subtracted from the pressure to be measured, then it is called a differential type of sensor.

## 4.2 Requirements of the pressure sensor

In this section some estimates of the required specifications of the sensor are given. Most of these values can be influenced by adapting the experimental set-up. They serve as a first indication for the suitability of a sensor.

**Sample frequency 100 Hz**

There is a notion that eddies of twice the size of a stone can produce the most effective pressure gradient for lifting a stone (see chapter 2). These eddies pass the stone with a certain velocity. The frequency required to distinguish these eddies can now be determined, if the approximate experimental conditions are estimated. A stone diameter of 2 cm and a flow velocity of 1 m/s are normal values for a critical flow velocity. This would mean that an eddy (of 4 cm) would pass in

0.04 s. A sample frequency of 50 Hz would detect this. Using a larger frequency range would give a good picture, so at least 100 Hz is required.

### Accuracy 1 N/m$^2$

A typical value for the root mean square value of the turbulent velocity fluctuations in turbulent, uniform flow is 10% of the mean velocity. This can be used to get an indication of the magnitude of the turbulent pressure fluctuations: $p' = \rho u'^2 = 0.01 \rho u_{ave}^2 = 10$ N/m$^2$, using $u_{ave} = 1$ m/s. For the detection of variations around this value an accuracy of 10% of this value, or 1 N/m$^2$, would be required. The stability of the sensor does not need to be very good, as high frequency fluctuations are to be measured. However, in order to obtain a good spectral estimate, the stability during about 10 minutes (one measurement) should be good. The mean pressure is also of importance for the stability of stones, but it is not essential to measure this pressure, as the main focus is on the fluctuating pressures.

### Measuring area 0.5 cm $\times$0.5 cm

In order to be able to correlate certain pressures at various places on a stone, a diameter of the sensing area significantly smaller than that of the stone is required, so with a stone of 1 or 2 cm, 0.5 cm is the maximum size. A $d^+$ of 19 (ca. 0.2 mm for the assumed conditions) would capture all turbulent frequencies, but this is not required, as the smaller scales (higher frequencies) do not influence the forces on the stones. The total size of the sensor should also be small (at least smaller than the stone of a few cm) in order to be able to place it in or near the stone.

### Water resistance

The sensor has to be resistant to water, as this is the medium in which the pressures will be measured. When a differential sensor is used, the reference side will be exposed to air.

### Range 2500 N/m$^2$

The range in which pressures will be measured depends on the type of measurement. An absolute type of sensor will also measure the atmospheric pressure, so this type will not be applied. Therefore a differential sensor will be used. In order to purely measure the pressure fluctuations, the reference pressure has to be equal to the local hydrostatic pressure, this will mean that extra facilities are needed to create a stable reference pressure. It is also possible to measure the hydrostatic pressure, of approx. 2000 N/m$^2$ (water column of 20 cm). As long as the accuracy is sufficient, the measuring range of a sensor can be larger. But as the accuracy is mostly a percentage of the measuring range, the range will have to be close to the required value. For the different sensors, the following ranges are required:

- absolute: 102500 N/m$^2$ (1025 mb)
- differential on air: 2500 N/m$^2$ (25 mb)
- differential with adapted reference pressure 500 N/m$^2$ (5 mb)

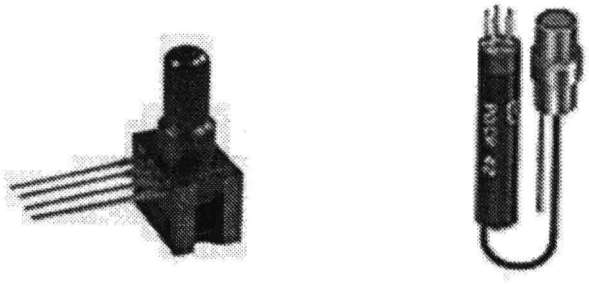

Figure 4.1: Selected pressure sensors, Honeywell (left) and Druck (right) (different scales, approx. 1:1).

## 4.3 The search

In total fifteen commercial companies that produce pressure sensors were contacted and asked whether they produced pressure sensors meeting the estimated criteria (appendix A). The types of sensors that work by measuring the displacement of a diaphragm by electro-magnetic or mechanical systems were either too slow, too big, or not accurate enough. A number of companies produced silicon dies that were small, had low ranges, and were accurate up to about 10 $N/m^2$ (0.1 mb) (*Honeywell, Novasensor, Analog*). These appeared to be semi-manufactured articles, intended to be installed larger assembled products, but they could be used. One company (*Druck Ltd.*) was found to produce a low-range sensor that was ready-to-use. *Bruel & Kjaer* also produced similar pressure sensors, only not in the required range.

There is also a material on the market, called *PiezoFlex*, that can be used as a pressure sensor without reference pressure. It is a 0.5 mm thick material on which pressure sensors can be etched with a different electrical resistance, that varies with compression. Whether sensors can be made this way that are small and sensitive enough is being investigated, although the sensitivity is expected to be insufficient.

### 4.3.1 Druck

The *Druck* sensor (type PDCR42, see appendix B) is a piezo-resistive type sensor. A Wheatstone-bridge is etched on the diaphragm, making it temperature-compensated. The sensor is cylindrical (5 mm diameter, 2.5 cm long) and made of steel. The diaphragm is placed at the outside of the sensor. The reference pressure is led through a thin tube –which is integrated in the wire– to the plug. It has a measuring range of 7500 $N/m^2$, a company-specified accuracy of 4 $N/m^2$ (0.04 mb), and seemed to be capable of fulfilling the requirements for the experiments. Before acquiring this sensor, it could be borrowed from *WL|Delft Hydraulics* to be tested in a flume. The results were encouraging enough to proceed with obtaining some of the sensors, in order to do more elaborate tests. The sensors from *Druck* cost approx. 4500,- guilders a piece.

### 4.3.2 Honeywell

The *Honeywell* sensor (type 24PCEFA1D, see appendix C) also is a piezo-resistive type sensor, although it is not temperature compensated. It has a 6 mm × 9 mm × 7 mm rectangular housing, with tube-connections that can be removed, as it is made of plastic (polyetherimide). The sensing diaphragm of 2 × 2 $mm^2$ is placed inside this cover. It has a measuring rang of 2500 $N/m^2$, and a company-specified accuracy of 14 $N/m^2$. The fact that the *Honeywell* sensor still has to be prepared for the measurements (it is not delivered water resistant, and it is not connected with electrical wiring or tubes for the reference pressure), also makes that it can be used in a more flexible way. The cost of the sensor is approx. 60,- guilders, which is a factor 100 less than the *Druck* sensor.

The *Honeywell* was chosen instead of other sensors that were not ready-to-use, because of the fact that it was the smallest and the measuring range fitted the present application best. Furthermore, some other sensors had steel tubes, and were therefore more difficult to process. Although some of the other ready-to-use sensors were temperature compensated, the temperature of the water was not expected to vary significantly during the experiments.

# Chapter 5

# Noise sources

## 5.1 Introduction

Chapter 6 deals with filtering techniques. Nevertheless, it is always better to reduce the noise in the signal than to filter it from the signal afterwards, as a filter never works perfectly. This is why a thorough study has been made on the noise sources that are present in the experimental facilities, both present and future. The results are described in chapter 8. In this chapter some general features of noise in wall pressure measurements are described.

The word noise normally is used for a random wide-band signal. However, the main noise sources in wall pressure measurements have a different character. These are caused by the vibration of the structure and by acoustical waves. They are narrow-banded, rather deterministic signals that are added to the wall pressure signal. Although these disturbances are not random wide-band signals, they are still referred to as noise in this report. Consequently, the term 'noise peaks' is also used. Another characteristic is that this noise has large spatial scales, so the pressure field caused by them can locally (throughout the measuring area) be regarded as spatially uniform.

These features offer us a few opportunities to determine whether this kind of noise is present or not. First of all, the narrow-band noise appears as a peak on the broad band turbulence signal. A narrow peak is very unlikely to originate from turbulence, so it is a clear indication. Secondly, the correlation of two pressure measurements, made with a fair distance, is high for the large-scale vibrational noise, and low for the smaller-scale turbulence. Coherence functions can be used to show this very easily (see ch. 8). Vibrations can also be measured directly with an accelerometer. Furthermore, much of the noise sources can be present without flow (and hence without turbulence) present, so that the frequencies of the noise can be measured directly.

Discriminating between vibrational and acoustical noise in the measured signal presents a problem, as they both have similar features and can originate from the same source. Vibration, however, can be measured by an accelerometer. In this way at least the correlation between vibration and the pressures at the pressure sensor can be determined, which gives some indication whether the source is accoustical or not. This is a difference between the paths along which noise reaches the sensor. For instance, noise created by a pump can reach the sensor by traveling through the building itself, or through the water. So, it is not only important to know the sources, but also to know the most important paths, if a noise free facility has to be designed. Wall pressure

fluctuations caused by vibration of the flume mainly occur at the natural vibration frequencies of the flume. These frequencies are excited by the various sources in the surroundings. These sources can be influenced, whereas the natural frequencies themselves can also be influenced.

In the case of wall pressure measurements the classic wide-banded random kind of noise is present as well: the sensors and amplifiers are not ideal, electro magnetic radiation affects the output voltage of the sensors, etc., so a certain broad-band low noise level is expected. This could be of importance, as only a small portion of the whole range of the sensors (5 $N/m^2$ on 2500 $N/m^2$) is used.

## 5.2 Possible sources

The noise level in the measured signal must be as low as possible. For this the sources of the noise must be known. Possible sources of disturbances that influence the signal are listed below:

- Electromagnetic:
  - frequencies caused by the AC power supply
  - frequencies of the monitor used for the data-aquisition system
  - lights (TL)
  - mobile phones (GSM)
- Vibrations in the surroundings:
  - inflow of water into the research facility
  - outflow of water from the research facility
  - gantry crane moving
  - pumps running
  - other flumes running
  - people walking/driving by
- Outside the lab:
  - construction activities
  - cars passing by
  - activities in the adjacent laboratory
- Flow related
  - short waves
  - long waves
- Sensor imperfections
  - temperature dependance
  - non-linearity

  - hysteresis
  - drift
- Amplifier stability
- Reference pressure (vibrating tube)
- Air pressure oscillations
- Acquisition and processing of data
  - discretisation of the measured signal

In chapter 8 the influence of these noise sources is described.

# Chapter 6

# Filtering Techniques

A number of filtering techniques are possible for dealing with the –mainly acoustical and vibrational– noise that is present in the measured pressure signal. Three techniques are described in this chapter. Furthermore, the application of the techniques to the first measurements of wall pressures on a smooth wall, as well as on an artificially generated signal, is described. For the analysis of the filters, the notation of Bendat & Piersol (1971) is mainly used.

## 6.1 High pass filtering

A simple way of eliminating noise is to ensure that the noise (peak) is present in an other frequency range than the signal of interest. When the peaks are in a lower-frequency range a high-pass filter can simply be used to remove the noise peak. Conversely, a low-frequency filter can be used when high-frequency noise is present. It is also possible to obtain a signal in the time domain this way. In figure 6.1 the premultiplied (variance preserving) spectrum of a wall pressure measurement on a flow with a free surface is presented. The variance in the measured signal is distributed over two separate frequency ranges(0.1–3 Hz and 3–250 Hz). The high-frequency fluctuations are caused by the turbulence pressures, and the low-frequency fluctuations probably by slightly instationary standing waves (see section 8.1). In this case the low frequency energy can be cut off from the signal by a high-pass filter without loss of much of the turbulence signal. It does result in the loss of some of the signal, so this procedure is not perfect. Especially for turbulence signals, which are very wide band signals, this approach is often not possible.

## 6.2 Difference method

A filter that is often used in measurements of wall pressures is the difference technique. It it suited for removing spurious pressures caused by structural and acoustical vibrations. An experimental set-up with two pressure sensors, mounted flush with the wall, having the same longitudinal position (in the direction of the flow) and a spacing in the lateral direction is used. For this technique it is required that the pressure signals, $s_i$, consist of a turbulent part, $c_i$, and a vibrational/acoustical part, $v_i$:

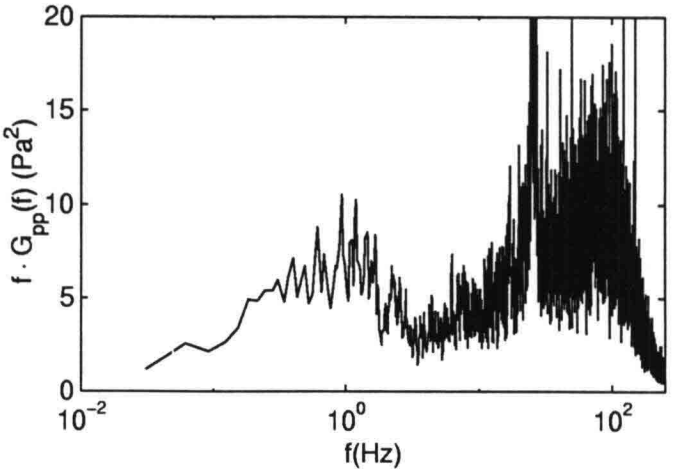


Figure 6.1: Premultiplied spectrum of open channel wall pressures, including low frequencies

$$\begin{aligned} s_1(t) &= v_1(t) + c_1(t) \\ s_2(t) &= v_2(t) + c_2(t) \end{aligned} \tag{6.1}$$

The filter is based on the fact that structural and acoustical pressure disturbances are uniform over relatively large areas, compared to the turbulence pressures. If the distance between two pressure sensors in a flume is large enough (at least the boundary layer height $\delta$), the turbulence pressures can be uncorrelated, while the vibrational/acoustical pressures can still be approximately equal ($v_1(t) \approx v_2(t)$). When these conditions are fulfilled, the two signals can simply be subtracted. This gives:

$$\Delta s(t) = s_2(t) - s_1(t) \approx c_2(t) - c_1(t) \Rightarrow G_{\Delta s \Delta s} \approx G_{c1c1}(f) + G_{c2c2}(f) \tag{6.2}$$

where $G_{ii}$ is the autospectral density of the signal $i$.

This result can be used as a filter that is able to determine the spectral characteristics if the two turbulence signals are statistically equal, i.e. measured at a similar position in the flume. In this case it simply follows that $\frac{1}{2}G_{\Delta s \Delta s}$ is equal to the autospectral density of one turbulence signal. However, the time trace is only obtained of the difference in pressures.

Luckily, the time trace of a difference in pressure can directly be used for examining stone stability, because only a pressure gradient can cause a net force on a stone, and a measurement of pressures at two different sides of a stone is representative for the pressure gradient over that stone. So, when the difference in pressure between two points on the stone is measured, then the vibrational noise is cancelled, and an estimation of the pressure gradient is obtained.

Although it is important to know the pressure gradients, it is still desirable to know the time trace of the fluctuating pressure at one point. With different flow processes at the different sides of the stone –for example a stagnation point at the front of the stone and vortex shedding at the back– it is useful to know the total pressure that is caused by the turbulence at a single point. This way the single processes can be studied in a better way. For instance, it can be seen directly

by which velocity sources the maximum pressures are caused. By using the difference filter this is not possible.

A problem could occur when using the difference filter for pressure measurements around a stone. If pressure sensors are placed at various locations around a stone, instead of at a fixed depth, it is questionable whether a fixed vibration gives the same pressures at the different sensors, because the water height ($\propto$ accelerated mass $\propto$ pressure) above the various sensors varies. This will make the difference filter not totally effective.

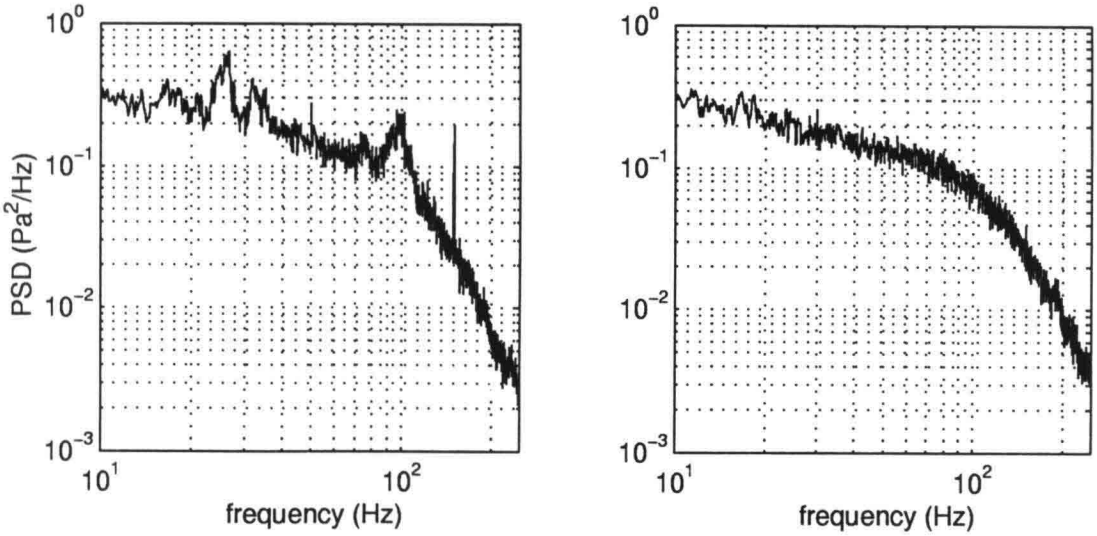


Figure 6.2: A power density spectrum of wall pressures, both unfiltered (left) and filtered with the difference filter (right)

**Performance of the filter**

The difference filter was shown to be functioning very well for the wall pressures that were measured. For the higher flow velocities, where the signal-to-noise ratio was relatively high, the few peaks created by vibrational/acoustical noise that were visible in the spectrum were attenuated. A sample plot for a measurement with a low noise-content is given in figure 6.2. At lower velocities still some vibrational/acoustical noise peaks remained in the spectrum. The noise apparently was virtually equal at both sensors, but not completely. Whether this will be the case for a varying bed topography (which will be used in the final experiments) is not sure.

## 6.3 The 'optimal filter'

The optimal filter was described by Naguib *et al.* (1996). It is based on the same set-up as the difference filter. However, in order for this filter to work, the noise at both pressure sensors does not have to be exactly the same. It does have to be correlated via a linear system.

The filter is described as:

$$c_1'(t) = s_1(t) - v_1'(t) = s_1(t) - \int_{\tau=0}^{\infty} f(\tau) s_1(t-\tau) d\tau$$
$$\int_{\nu=0}^{\infty} f(\nu) R_{s1s1}(\nu - \tau) d\nu = R_{s1s2}(\tau) \tag{6.3}$$

where $c_1'$ is the filtered turbulence signal, $v_1'$ is the filtered noise signal, $R_{s1s2}$ is the correlation function of the two measured signals, $f$ is the filter function, $\tau$ and $\nu$ are time lags, and $R_{s1s1}$ is the auto correlation function of one of the measured signals, $s_1$.

The method was reported to be working very well by Naguib *et al.* (1996), who used a discretised form of equation (6.3) for calculating the filtered signal directly in the time domain.

Although the calculation is possible in the time domain, it requires greatly increasing computing times for increasing filter lengths. This is caused by the fact that a square matrix has to be inverted in order to determine the discrete filter function, which has the dimension of the filter length. It is also possible to execute the filter in the frequency domain, which significantly decreases the computation time required. The filtering in equation (6.3) is equivalent to the following filter in the frequency domain, which can be computed much faster:

$$F_{v2v2}' = H_{s1s2} F_{s1s1}$$
$$c_2'(t) = s_2(t) - \int_{-\infty}^{\infty} F_{v2v2}' e^{2\pi f t i} df \tag{6.4}$$

where $F_{v2v2}'$ is the Fourier transform of the estimated noise component, $H_{s1s2}$ is the frequency response function of the two signals, and $F_{s1s1}$ is the Fourier transform of signal $s_1$.

The power spectrum can be filtered in the following way:

$$G_{c1c1}' = (1 - \gamma_{s1s2}^2) G_{s1s1} \tag{6.5}$$

$G_{c1c1}'$ is the estimate of turbulence signal $c_1$, $\gamma_{s1s2}^2$ is the coherence function of the two measured signals, and $G_{s1s1}$ is the auto spectrum of one of the measured signals, $s_1$.

### Performance of the filter

The equations (6.5) and (6.4) are taken from Bendat & Piersol (1971). The term 'optimal' is presented by them, as it is shown by a least-squares procedure that this gives the optimal estimation of the signal, in the sense that the integrated square difference between the real and the filtered signal is minimal. The filter is derived for systems with two linearly correlated signals with random noise at the output. However, for our application the correlated part, which is called the 'signal' by Bendat & Piersol, is defined as the (vibrational) noise, and conversely their uncorrelated 'noise' part is the turbulence signal we need. Further, there is also uncorrelated turbulence signal added to the input of the linearly correlated noise. This influences the validity of equation (6.5). Below it is shown that even for a perfect measurement set-up the optimal filter is not perfect.

The performance of the filter can be studied by using the Fourier-transformed version, and when $v_1 = v_2$, and $c_1$ and $c_2$ are uncorrelated and statistically equal signals ($G_{c1c1} = G_{c2c2} = G_{cc}$), equation (6.5) can be rewritten as (Bendat & Piersol, 1980; Naguib *et al.*, 1996):

$$\frac{G_{cc}'}{G_{cc}} = 1 + \frac{1}{1 + SNR} \tag{6.6}$$

where $SNR$ is the energy-based signal to noise ratio, $G_{cc}/G_{v1v1}$. This equation shows that there is always a part of the noise left, and that the noise on the signal cannot be totally attenuated after filtering. Naguib *et al.* (1996) argue that the noise is always reduced by more than 3 dB, which is practically true. However, a very large noise peak in the original signal will still be present in the filtered spectrum as a peak. For a relatively high noise level ($SNR \to 0$) the relative reduction of the vibrational component increases, but the estimated turbulence signal is still overestimated by a factor of about 2, which is 0.3 decades on a log scale.

The filter was tested to measurements of wall pressures. This was done in the frequency domain. It can be seen from an example of an auto-spectrum in figure 6.3 that noise peaks are reduced after filtering, but still remain present in the signal. This is in agreement with equation (6.6).

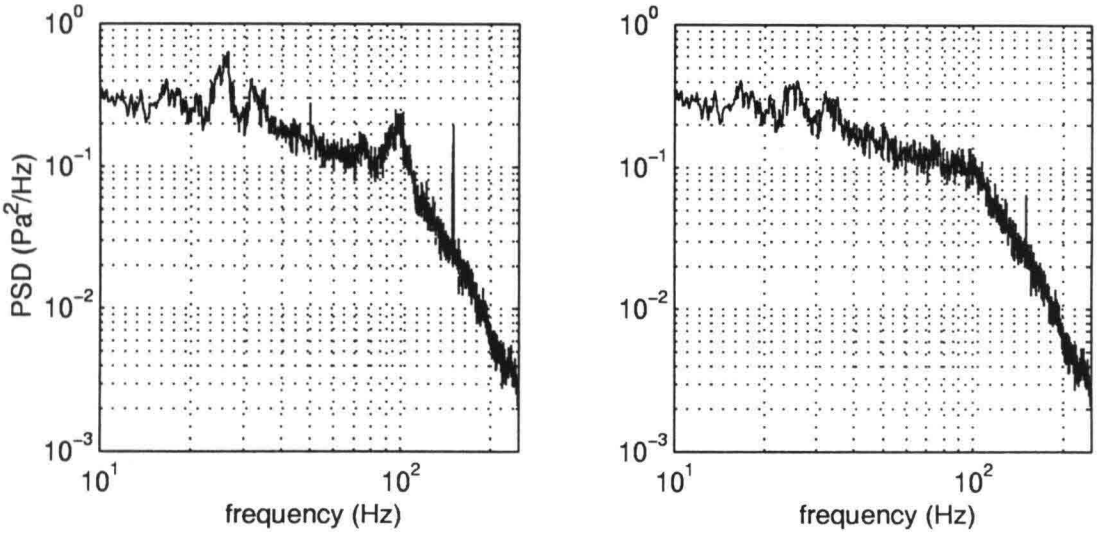


Figure 6.3: A power density spectrum of wall pressures, both unfiltered (left) and filtered with the optimal filter (right)

The filter was also applied on a simulated signal. This has the advantage that both the real "turbulence" and the real "vibrational" input signals are exactly known. The original signals can therefore be compared directly with the filtered signals. This can be done in both the spectral and the time domain. For the artificial turbulence signal an autoregressive model was used (Waele), which creates a spectrum with a $f^{-1}$ behaviour for the mid-frequencies, and a higher fall off for the higher frequencies. This is similar to the behaviour that is found in wall pressure spectra. For the vibrational component two sinusoidal signals with a slight phase difference are used. This creates a beat in the signal, and is characteristic for a forced vibration. The vibration appears in the spectrum as a peak on the wide band turbulence spectrum. The respective spectra (not shown here) are equal before and after filtering, except for the fact that the noise peaks have reduced in size. Unfortunately, like in the real experiments (figure 6.3), they have not disappeared totally.

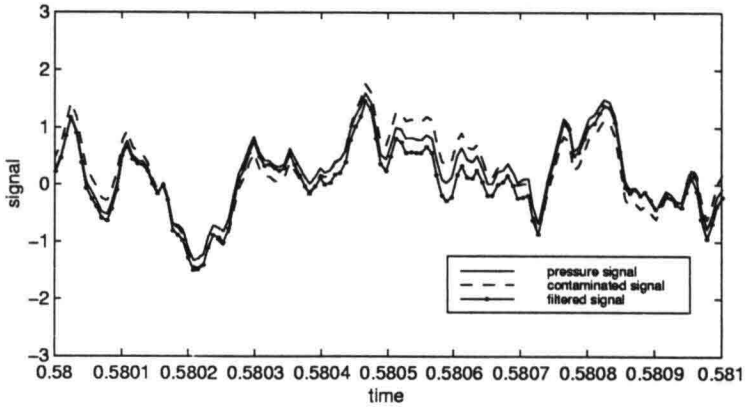


Figure 6.4: An artificial wall pressure signal, including contaminated signal and signal filtered with optimal filter

Of course the idea comes into mind of using the filter a number of times on the same signal. This seems to work satisfactorily the first time the filter is repeated, as the r.m.s. difference between the original signal and the filtered signal decreases. However, after consecutive repetitions there is no noticeable change anymore, even a deterioration. Filtering for two consecutive times seems to be the best option until now. In figure 6.4 the signal after using the filter once is shown. In general the filtered signal is closer to the original signal, but instances can be found where this is not the case.

A great advantage of the optimal filter is the fact that it can be used in the time domain. The conclusion about the effectiveness of the optimal filter is for the moment that it can help to "polish" the signal. The filtered signal will resemble the turbulence signal more, but the resemblance is not perfect. Other ways of using it can still be tried, and contact has been made with the authors of the original article about the application of the technique.

# Chapter 7

# Experimental set-up

Several experiments have been done with the pressure sensors in order to learn about their performance and the noise caused by the experimental facility. The configuration, the apparatus, the data-processing, and the relevant parameters are described in this chapter.

## 7.1 Flow conditions

The experiments under flow conditions have been executed in a flume with a hydraulically smooth bed. The bed had to be raised in order to create space for mounting the pressure sensors. The bed was constructed with a plastic cover on top of a bed of sand and cement. The flume, which had a horizontal plane bed, is shown in figure 7.1. The total length of the flume is approx. 15 m, and the width is 0.5 m. Two pressure sensors were mounted flush with the bed in a removable plate. In this way the sensors could easily be replaced. They had an equal longitudinal position (in the flow direction), and a transverse spacing of 17.5 cm. The water was led into the flume by a diffusor that was situated under water in order to decrease the vibrations caused by the inflow. The water level in the inflow section was raised by installing a perforated plate between the inflow section and the rest of the flume, in order to decrease the vibrations as well. Floating plates were put near the inflow, and were also tried near the measuring section, in order to attenuate the surface waves, which did not work very well. The water level in the outflow section was raised as high as possible. This decreased the height over which the water fell, also reducing the vibrations.

Pitot tubes were placed at three positions to measure the water level. The discharge was determined applying an orifice plate in the inflow pipe. Both types of pressure sensor were used.

### 7.1.1 Experiments

First the flow conditions in the flume had to be optimized. The inflow and outflow sections were adapted such that the flow was as smooth as possible. Once the flow conditions were satisfactory, various flow conditions were tried. It became clear that the wall pressure fluctuations increased more than the vibrations, when increasing the discharge. A maximum discharge of 76.5 l/s was used, which gave the highest wall pressures. Table 7.1 lists the main experimental parameters, where $Q$ is the discharge, $h$ is the water depth, $\bar{u}$ is the average velocity, $u_*$ is the friction velocity,

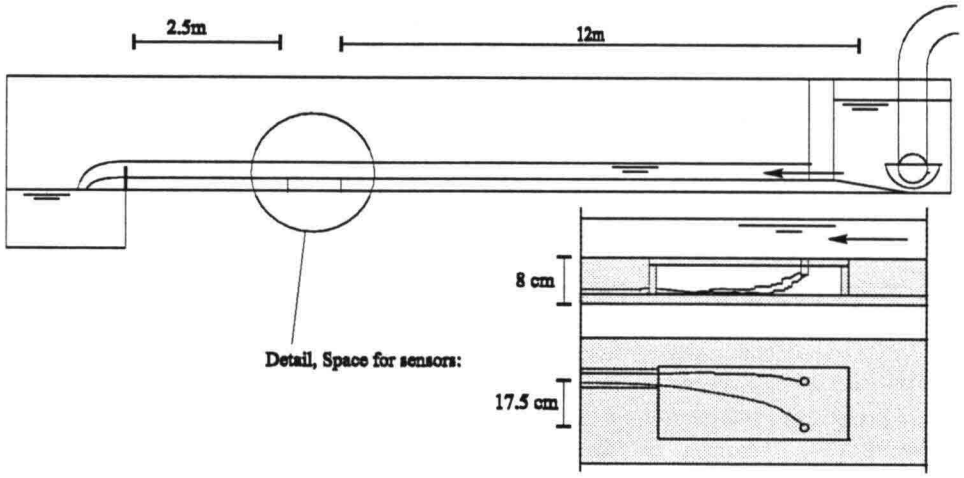


Figure 7.1: Flume used for experiments

| $Q$ $(l/s)$ | $h$ $(m)$ | $\bar{u}$ $(m/s)$ | $u_*$ $(m/s)$ | $Re$ (-) | $\overline{p'^2}^{\frac{1}{2}}$ $(N/m^2)$ | $\overline{p'^2}^{\frac{1}{2}}_{noise}$ $(N/m^2)$ |
|---|---|---|---|---|---|---|
| 59.5 | 0.207 | 0.58 | 0.028 | 118000 | 2.70 | 1.70 |
| 59.5 | 0.159 | 0.75 | 0.036 | 118000 | 4.18 | 1.09 |
| 59.5 | 0.141 | 0.85 | 0.040 | 118000 | 4.90 | 0.81 |
| 76.5 | 0.166 | 0.92 | 0.043 | 152000 | 5.67 | 0.93 |

Table 7.1: Experimental parameters

$Re$ is the Reynolds number, $\overline{p'^2}^{\frac{1}{2}}$ is the r.m.s. of the filtered TWP, and $\overline{p'^2}^{\frac{1}{2}}_{noise}$ is the estimated r.m.s. of the noise.

### 7.1.2 Data processing

The method that was used for visualising the results was mainly by making variance density spectra. A typical measurement had a duration of 5 minutes, and a sample frequency of 500 Hz, resulting in a little more than $2^{17}$ samples. This way a spectrum could be made with a Nyquist frequency of 250 Hz. A measurement was windowed with a Hanning window of $2^{12}$ samples ($\approx 8s$) with a 50% overlap, giving: $2^6 - 1 = 63$ separate windows for averaging. These spectra give a good picture for frequencies higher than 1 Hz. For spectra that were meant to examine lower frequencies, longer window lengths were used.

## 7.2 Stagnant water

Three different pressure sensors were mounted next to each other in a container with water. One *Druck* pressure sensor with a pinhole, one *Druck* sensor without a pinhole, and a *Honeywell* sensor with a pinhole. The *Honeywell* sensor could not be constructed without a pinhole. The calibration factor could be determined very accurately by adding volumes of water that created small increases of the water level. The linearity could also be checked by this procedure. The calibration factor was determined several days in a row in order to study the long term stability. The temperature influence was also studied with this set-up, by heating the water.

## 7.3 Simultaneous vibration and pressure measurements

Direct vibration measurements were also executed. For the vibration measurements a *Brüel & Kjær* (type 4367) accelerometer was used.

Most experiments were done with the flume at which the wall pressure measurements have been done, while it was running. WPF measurements were executed simultaneously to the vibration measurements, making it possible to examine the coherence between the spurious pressures and the vibrations. The flow in the flume had a relatively high discharge and a large water depth. The high discharge and large water depth caused more vibrational noise, and the large water depth kept the velocity limited, which resulted in moderate TWP levels. Some experiments were done without flow in the flume in order to see the pure effect of vibration, without acoustical influences.

Other tests were executed on several other flumes with the pumps running. In this way an idea could be obtained of the presence of vibrations in the laboratory and about the characteristics of other flumes to be used for future experiments.

Finally some measurements were executed with a transient load. This was accomplished by dropping a fixed weight from a fixed height near a specific place/flume, and consequently measuring the vibrations, both of a flume and of the floor. The ratio of intensities of the vibrations of the flume and the floor can give an idea of the gain factor between vibrations of the floor and flume.

# Chapter 8

# Results

The main aim of the present investigation was to investigate the possibility of measuring wall pressures. The first requirement for measuring wall pressures is having suitable pressure sensors at one's disposal. The second is the requirement of an experimental facility without disturbances. In this chapter the possible sources of spurious signals, both by vibrations, and imperfections of the sensors are discussed. Some attention is paid to the wall pressures, which are used as a check for the pressure sensors and the experimental facility.

## 8.1 Short waves

In a flow with a free surface waves are often present. During the smooth bed measurements they were indeed observed. Flow velocities had to be very high in order to generate high levels of wall pressures. This also led to high Froude numbers, which caused increased surface slopes. The joints between the successive sections of the flume are not totally smooth, hence waves were induced. Fairly large standing waves (wave length, $L \approx 20$ cm) were observed, which were slowly oscillating back and forth. Only in the low frequency range ($< 10$Hz), the TWP are affected by the free surface waves. This is derived in the rest of this section.

Waves that propagate with varying angles to the flow direction, have a maximum apparent frequency when moving in the direction of the current. The maximum apparent circular frequency for a certain wavelength becomes:

$$\omega' = (c + u_{||})k \tag{8.1}$$

where $\omega'$ is the apparent frequency, $c$ is the wave celerity, $u_{||}$ is the flow velocity, and $k$ is the wave number.

From the dispersion relation for free surface waves including the effect of surface tension, the bed pressure can be obtained. It can be rewritten as:

$$|\overline{p'^2}| = \left(\rho \frac{g + \frac{\sigma}{\rho}k^2}{\cosh kh}\right)^2 |\overline{\zeta^2}| \tag{8.2}$$

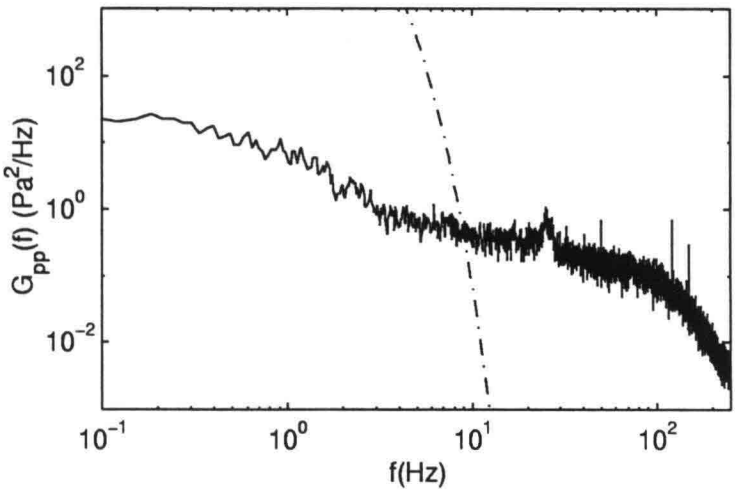


Figure 8.1: Wall pressures for open channel experiment (–), including maximum influence of surface waves (–.)

where $p'$ is the varying pressure, $\sigma$ is the surface tension, $\zeta$ is the surface elevation, and $h$ is the water depth. The term between brackets in the right hand side of eq. (8.2) denotes the gain factor from the spectrum of surface elevation fluctuations to the spectrum of pressure fluctuations caused by the waves.

If the surface elevations are assumed to be caused only by waves of a single frequency the spectrum of the wave energy becomes a delta function, with variance $\frac{1}{2}a^2$, where $a$ is the wave amplitude. The corresponding pressure spectrum is a delta function, of which the surface area (variance) is computed by eq. (8.2). This delta function appears in a discrete spectrum as a spike with the height of this variance divided by $\Delta f$ (bandwidth resolution), which in turn gives the maximum possible level of the wave-induced pressure spectral level for this frequency, $f$. In the flume a maximum surface elevation fluctuation of about 0.5 cm was observed at a single point. When one combines all the maximum spectral levels that are possible for this wave amplitude, one obtains an approximation of the maximum possible contribution of the short waves to the bed pressure fluctuations at each frequency. This approximation probably is much too high, as the bandwidth of the wave-induced pressures is probably larger than $\Delta f$.

In figure 8.1 a WPF spectrum is plotted for a flow velocity of 0.92 m/s, and a water depth of 16.6 cm. In the same graph the line of the maximum possible influence of waves is depicted. Above this line no influence of waves is expected of surface waves on the WPF. This shows that at frequencies higher than 10Hz, where the maximum possible influence by waves is lower than the TWP-spectrum, waves cannot be expected to have a significant influence on the wall pressures. But at low frequencies they can –and probably do– cause significant wall pressures. The increased level of the pressure spectrum in the frequencies lower than about 3 Hz –which is better visible in the premultiplied plot of figure 6.1– appears suspicious, and cannot be ascribed to turbulence fluctuations. The pressures in this frequency range are also highly correlated, which is another indication that this might be wave-induced pressures.

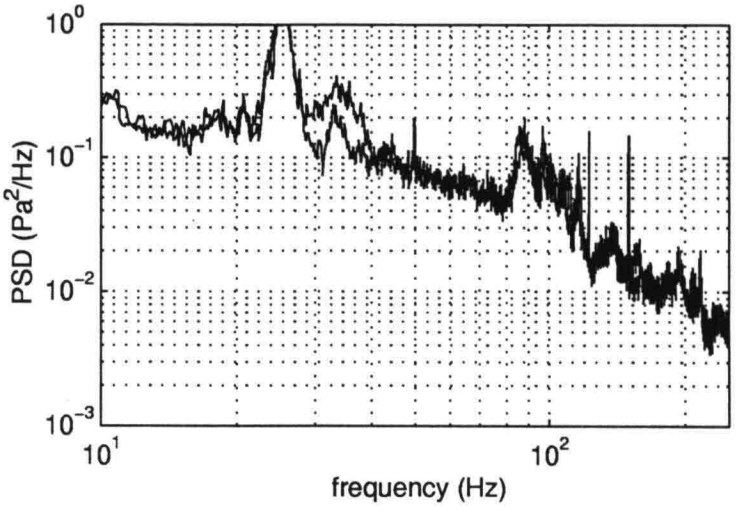


Figure 8.2: Spectra of two experiments with equal flow conditions, but changed outflow: lower line with higher water level in outflow

## 8.2 Long waves

An estimation of the period of long waves can be made according to: $2L/\sqrt{gh}$: half a wave length is present in the flume. Due to the length of this flume the period is in the order of 20 seconds. This is out of the frequency range that is of importance. In the transverse direction of the flume this could be an issue. A period of about 0.8 s can be expected. For the high flow velocities that will be used, this is also out of the range of interest.

## 8.3 Natural frequencies of flume

Two dominant low frequency noise peaks (around 27 Hz and 34 Hz) are present in the vibration spectra of both the outflow section and the flume bottom, see figures 8.3 and 8.4. For both peaks the coherence between the pressures on the bed and the vibration of the flume on the one hand and the outflow on the other hand was also nearly one. Therefore the exact path and/or source are difficult to determine.

It was clear that the violent outflow of the water, by means of a weir, generated a lot of noise in the signal. The outflow section consisted of metal plates without stiffening. The plates can vibrate freely, thereby creating a lot of noise. In figure 8.2 the power spectrum of two measurements with exactly similar flow conditions are shown. Only the water level in the outflow was altered, so the vibration was less during the second experiment. One peak was clearly decreased, while the rest of the spectrum remained the same. Therefore this resonance peak (around 34 Hz) clearly originates from the outflow-section.

The other peak is probably caused by the vibration of the flume. This is supported by the fact that when the flume was struck, the first peak (27 Hz) of the response spectrum was highest, and when the outflow was struck, the second peak (34 Hz) of the response spectrum was highest.

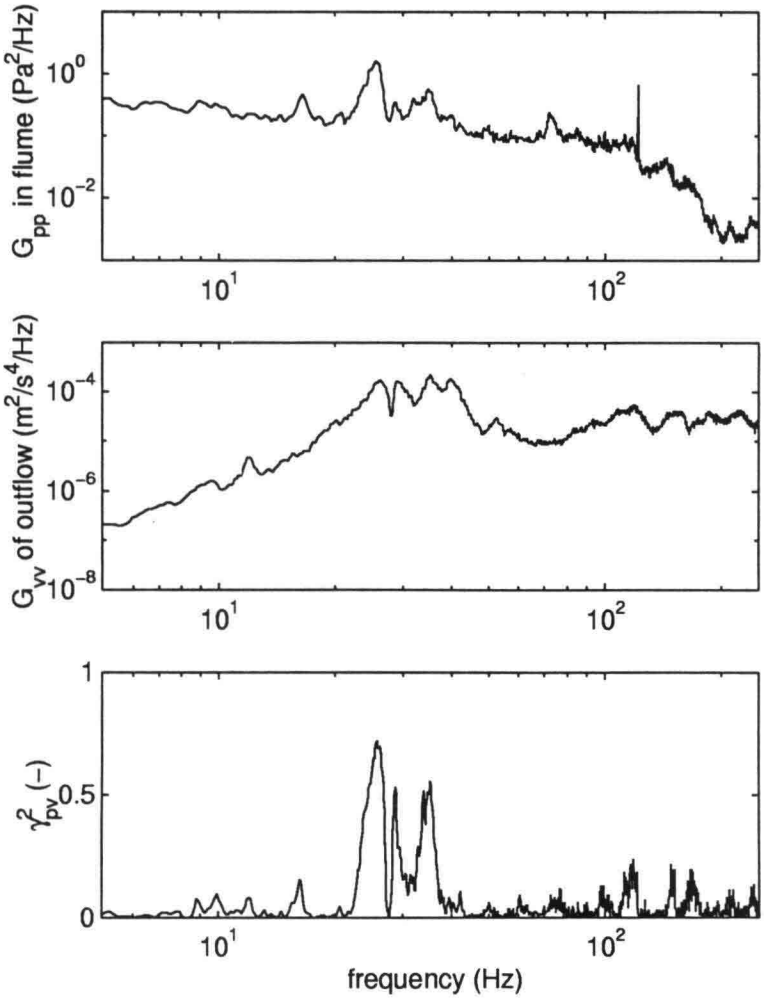


Figure 8.3: Power spectrum of wall pressures (top), accelerations of outflow (centre), and coherence function of both (bottom). Experiment with moderate flow.

The close link between the accelerations of the flume bottom and the wall pressures is shown in figure 8.5. Both spectra almost totally coincide except for some peaks. The pressure that would be caused by the acceleration of the water column is plotted by the lower line, which is determined by $\rho g$ times the measured acceleration at the flume bottom. There is still a slight difference between both peaks, also when the turbulence is removed, which could be explained by various facts. The question remains whether the vibration causes the pressures, or conversely: the pressure causes the vibration. Still it seems very unlikely that the vibration is caused by acoustical pressures, and that the bed is vibrating that much in the 27 Hz mode, without the mode being its own natural frequency. Therefore it is concluded that most high frequency noise originates from vibration.

## 8.4 Vibrations due to pumps

The vibrations of the pumps are present in the signals at certain frequencies. When measuring the vibrations of the pumps a distinct peak was found at 122 Hz, see figure 8.6. This peak can still be found in the pressure signal for the situation without flow in the flume. If there is flow in the flume, the peak is much larger. This would indicate that the vibrations introduces sound, which propagates through the pipes. It is a narrow peak, so it does not disturb the character of the broad band turbulence signal. The phase of the vibration is also very constant, so it is feasible to filter the vibration from the signal. Another large peak is present at 24.4 Hz in the vibrations of the pump. This peak does not create the vibration peak present in the pressure signal, as there is no coherence between this vibration and that of the wall pressures.

## 8.5 Electromagnetic disturbance

It has become clear that electro magnetic radiation influences the measurements. Direct current amplifiers –which are used for piezo-electric sensors– are known to be affected by electro magnetic radiation, so this is the most likely cause of disturbances from this radiation. A 50 Hz and a 150 Hz peak were always visible in the signal. The DC input of the sensor was checked and did not contain the 50 and 150 Hz peaks, so they are probably caused by radiation. The pressure sensors were permanently shielded by the water that was connected to earth, so not much interference is expected from this. When the monitor of the data-aquisition system was switched on, several extra spikes appeared in the spectrum (mainly 32.5 and 65 Hz). Therefore the monitor was kept switched off during experiments. The 32.5 and 65 Hz peaks caused by the monitor were now absent in the spectra. Also the overall noise variance was significantly reduced. The radiation mostly is present in very thin peaks in the spectrum, so it does not give much problems in analysing the results. Although, when a mobile phone was used in the vicinity of the test set-up, the signal was totally unusable.

## 8.6 Turbulence wall pressures

The measurement of turbulence wall pressures was used to test the pressure sensors in a real situation. Figure 8.7 presents the auto spectra of the TWP as measured at increasing flow velocities, plotted in two ways: the log-log plot shows the trend of the spectra for every frequency clearly, and in the premultiplied semilog plot the area under the plot still represents the variance. The

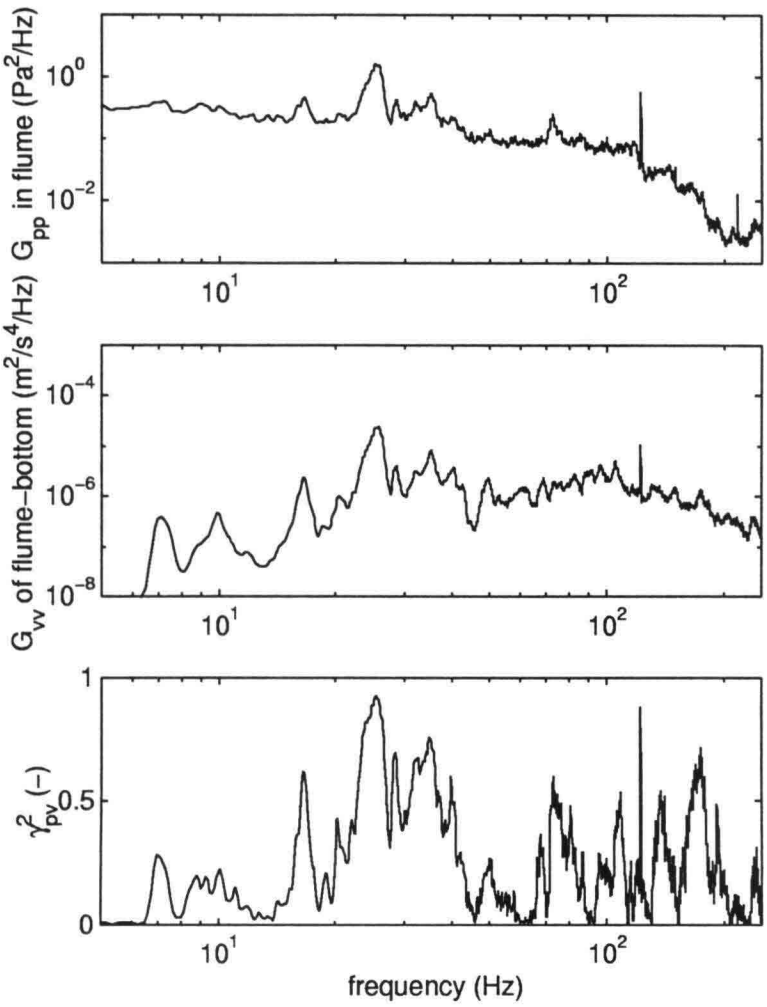


Figure 8.4: Power spectrum of wall pressures (top), vertical accelerations of flume bottom (centre), and coherence function of both (bottom). Experiment with moderate flow.

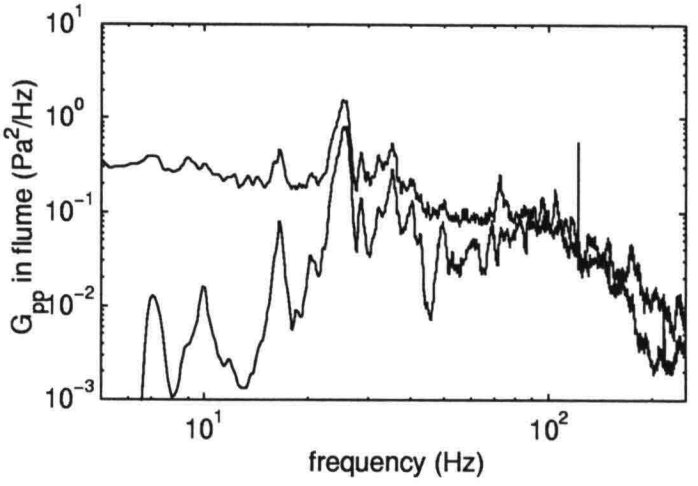


Figure 8.5: Power spectrum of pressures, and estimated pressures from acceleration via $\overline{p'^2} = (\rho h)^2 \overline{a^2}$ (lower line)

magnitude of the TWP obviously increases with increasing flow velocity, and the frequency range with the highest contribution to the variance shifts to the higher frequencies. Both trends can be expected. It can also be seen from figure 8.7 that the lower velocities have a relatively high noise level. For these conditions the irregular spectral features, corresponding to vibrational/acoustical noise, are dominant over the turbulence signal. This is most clearly seen for the measurement with the lowest bed friction (and corresponding lowest velocity). This spectrum is therefore omitted in figure 8.8, where the pressures are scaled. For the high flow velocities not yet all the variance is captured with a frequency of 250 Hz, which can be seen from the variance preserving (pre-multiplied) plot, which is cut off before the spectrum has reached a negligible level. But higher frequencies will not affect stone stability.

In the left plot of figure 8.8 the wall pressures on the bed are presented, scaled on inner flow variables. Mainly the high-frequency ($\omega^+ > 0.3$) and overlap-frequency ($100\nu/u_*\delta < \omega^+ < 0.3$) ranges (Farabee & Casarella, 1991) are depicted in the plot. They should collapse for $\omega^+ > 0.02.$, which they do. The shape, and the frequency regions are in agreement with the other research. Only the level of the overlap region does not agree. This level also differs for both other researches. The difference between the other two researches in the plot could be due to the fact that the filter used by Gravante *et al.* (1998) is expected to overestimate the spectral density at frequencies with a low signal-to-noise ratio by 3 dB (see chapter 6), which is approximately the amount with which their results are higher than the present results.

The right plot of figure 8.8 presents the pressures scaled on outer flow variables. Whether the pressures will coincide with the other research for the outer variables is uncertain, because wind tunnel experiments with a developing boundary layer are of a different nature than the present free-surface flow. For the length scale the water depth is used instead of the boundary layer height (where $\bar{u}(z) = 0.99\bar{u}_\infty$).

The pressures measured during the present research should collapse for values of $\omega^o < 2000$, which seems to apply. They should coincide with the results from previous research at the mid

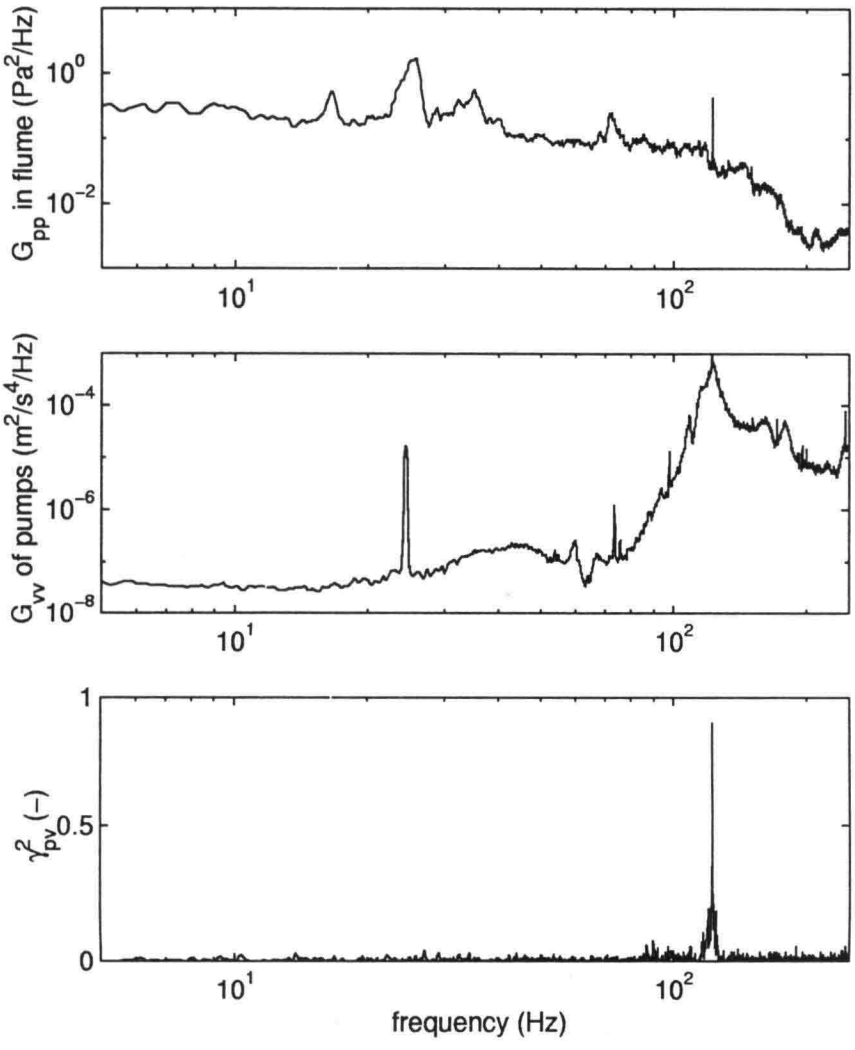


Figure 8.6: Vibrations caused by pump, during moderate flow

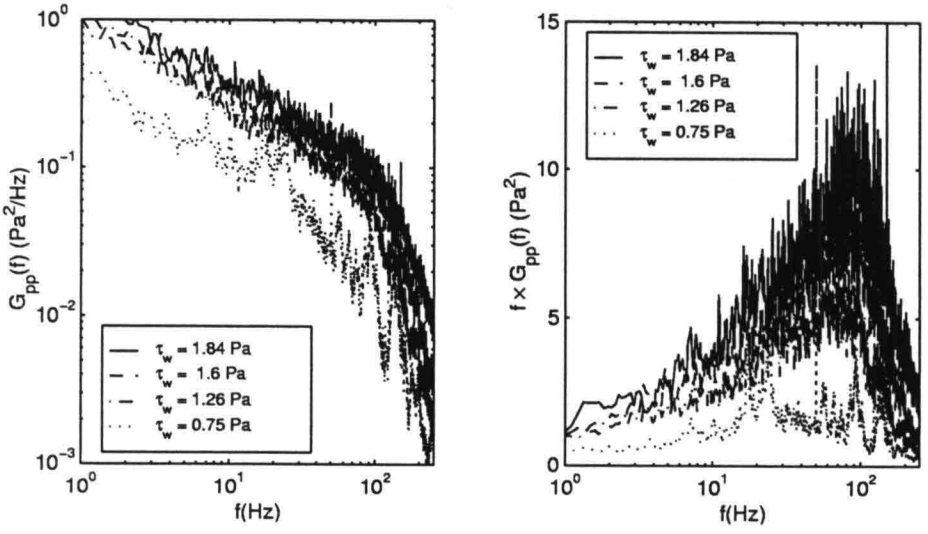


Figure 8.7: Power spectrum (left) and premultiplied spectrum (right)

frequencies $\omega^o < 100$. As expected, the non-dimensional pressures do not really coincide with the other measurements for the mid-frequencies. For frequencies higher than the maximum at $\omega^o > 50$ they coincide, but this maximum is not present in the present results.

## 8.7 Sensor characteristics

### 8.7.1 Frequency effects

The natural frequency of both sensors is several kHz. The response of the sensor is therefore flat. In other words, no resonance of the sensor diaphragm will occur in the experiments under consideration. The pinhole could cause some troubles. Although, as water is hardly compressible, there will be no effect of resonance of sound waves in the cavity (a few mm deep), which may be a problem with air flows. The compliance of the sensors (the volume of displaced water per pressure change)is not stated in the specifications. The compliance of a similar transducer (*Baxter*) was only $2 \cdot 10^{-6}$ mm/Pa. Therefore, if the sensors have a compliance of similar magnitude, no resonance or damping will be expected. However, if long and flexible tubes would be used to lead the pressure to the transducer, that could pose a problem regarding the frequency response.

In the high frequency range a slight difference between the *Druck* and the *Honeywell* sensors is noted. This is probably caused by noise due to imperfections in the sensor or amplifier, see section 8.9.

### 8.7.2 Spatial resolution

Spatial-averaging effects only occur when sensors are not small compared to the eddy-size. Because the sensors are going to be placed inside the stones, the sensor area is automatically small enough

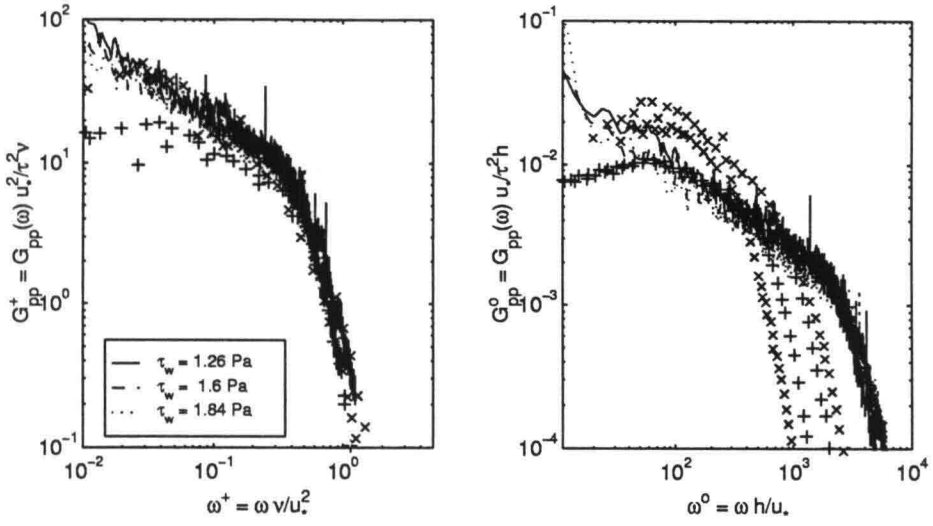


Figure 8.8: Spectrum scaled on inner (left) and outer (right) parameters, including wind tunnel results, +: Farabee and Casarella (1991), ×: Gravante *et al.*(1999)

to capture all relevant length scales; only the eddies that are in the order of magnitude of the stones contribute significantly to the forces on the stones. The small size of the sensor area also implies that the total force on the stone is not known. The maximum dimensionless diameter of the pinhole (actual diameter, $d = 1mm$) used for the smooth wall experiments was $d^+ = u_* d/\nu = 43$. This is very close to $d^+ = 19$, at which all turbulent length scales of the wall pressures are captured (Schewe, 1983; Gravante *et al.*, 1998). So this aspect poses no problems.

## 8.8 Temperature dependence

The water temperature is fairly constant during an experiment. The water temperature in the laboratory was observed to be constant within at least 0.1°C during the time of one experiment. It was not measured with greater accuracy. For different experiments the temperature did vary from 18–20°C. The temperature influences the offset of the sensor, but not the calibration factor, which can only be harmful if the temperature changes during an experiment. This could happen when water is heated in a pinhole by the sensor itself, and the heated water is advected from the pinhole in an intermittent way. The sudden changes in voltage that were observed sometimes could be caused by this effect.

It is clear that the temperature of the water has to be measured during the experiments and has to be kept at a constant level. Time signals must be checked on suspicious fluctuations.

## 8.9 Background noise

### 8.9.1 General

Background noise is present in the signal. The source of this noise can be imperfections of the sensors, electro magnetic radiation, or imperfections in the amplifier. Discretisation was not the cause (see8.9.2), even for the *Druck* sensor, which has a relatively large measuring range. As the *Druck* sensor has a larger range than the *Honeywell* sensor, its calibration factor (Volts to Pascals) is higher, therefore the disturbance of the measured signal is relatively larger. It can be seen that for high flow velocities the pressures are sufficiently higher than the background noise of the *Honeywell* sensor, but that the high-frequency fluctuations of the *Druck* sensor are influenced by the noise. Two kinds of amplifiers were tried, but the noise level did not alter significantly.

### 8.9.2 Discretisation

The fact that the measured signal is digitised by a 12-bit quantiser introduces an error, called discretisation noise. For both the *Honeywell* and the *Druck* transducer this did not interfere with the accuracy of the measurements.

It can be assumed that the discretisation error is uniform, with a variance of $\frac{1}{12}q^2$, where $q$ is the difference between two quantisation levels. When a signal is digitised by an $n$-bit quantiser, $q = r/2^n$, where $r$ is the range of the sensor in Volts . When the digitised signal is analysed by means of a variance density spectrum –keeping in mind that the spectral distribution of white noise is constant– then the variance is spread out over the entire frequency domain, from 0 to $f_{ny}$. This gives the following relation for the spectral level added by the quantisation:

$$G_{qq} = \frac{\frac{1}{12}q^2c^2}{f_{ny}} \tag{8.3}$$

where $c$ is the calibration factor. A broad band spectrum that has a decreasing energy level at higher frequencies, will have a gentle transition from the original slope to a horizontal line, determined by equation (8.3).

## 8.10 Long term stability

The stability of the sensors was tested by measuring the calibrating factor a number of times. This was accomplished by varying the water level a fixed amount, and measuring the change in output voltage of the sensors. The mean pressure did not appear to have an influence on the calibration factor. Over periods of a day, the offset changed in the order of 10 N/m$^2$. As the processes studied are not that slow, this is no problem. On shorter scales the offset seems constant, although sometimes a jump is seen in the offset. This jump can be due to the amplifiers. The disturbance can be recognised in the time-histories, and the good measurements can be selected.

When the pressure was changed suddenly by a fixed amount, the *Druck* sensor was seen to go to its equilibrium position more slowly than the *Honeywell* sensor. This can be seen in figure 8.9. This behaviour of the *Druck* sensor could be caused by the small tube for the reference pressure, which is smaller than a mm. This tube delays the air flow of the reference pressure.

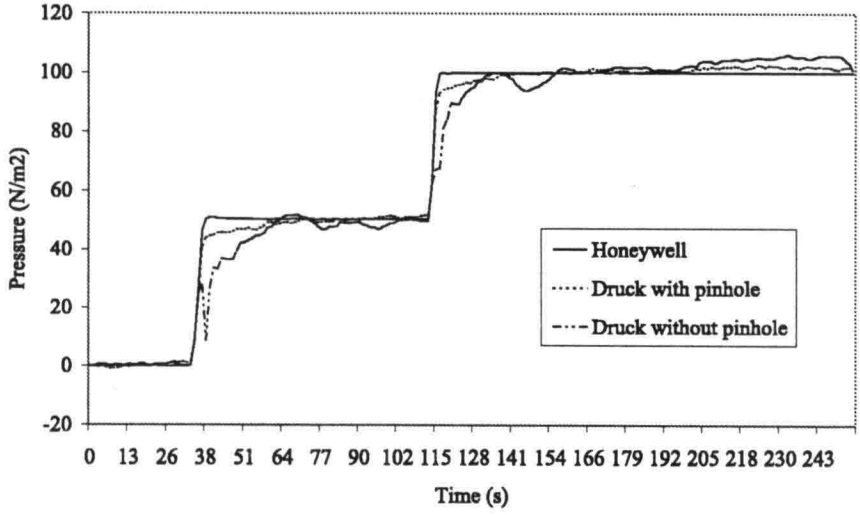


Figure 8.9: Example of calibration curve, scaled signal of three pressure sensors, after increasing water level two times

## 8.11 Reference pressure

The reference pressure (atmospheric pressure) can also change. But it is thought that this will not have a significant influence – especially for lower frequencies– as it is present at both sides of the diaphragm of the sensor.

However, when installing the sensors, care must be taken that the tube for the reference pressure is not vibrating itself. This clearly does influence the measurements. When one touched the tube, this clearly influences the measurements. For the present measurements the reference pressure was led through a pipe of 3 m length in the flume. When the reference pressure tube is vibrating, this could lead to extra noise in the signal. There was no way of finding out what the relative influence of this effect was.

# Chapter 9

# Conclusions

**Ability of pressure sensors to capture turbulence pressure fluctuations**

The pressure sensors seem to work satisfactorily regarding the accuracy and the frequency range they can cover. The stability of the sensor is not clearly known yet, but seems satisfactory. The vibrations from the surroundings of the flume influence the low and high-frequency parts of the pressure fluctuation spectrum obtained from the test measurements. Short waves influence the lower frequencies.

**Choise of sensors**

Of the two types of pressure sensors tested, the *Honeywell* sensors are found to be more precise, as their range is better suited for the present application. They also seem to be more stable than the *Druck* sensors. Furthermore, they can be used in more versatile ways. On the one hand because the cover is made of plastic, which can be processed easily, on the other hand the low costs make it possible to use a sensor for only one application and subsequently regard it as lost. Therefore the experiments will be executed with these sensors. One *Druck* sensor will be used, to check the pressure statistics at one point.

The temperature of the water must be kept constant, as the *Honeywell* sensor is influenced by it. The sensors will have to be calibrated before and after each experiment in order to determine the exact calibration factor for that experiment.

**Noise**

For the present flume two vibrational noise peaks were present in the low-frequency range of the pressure signal. They were caused by vibration of the flume and the outflow section. High-frequency disturbances are clearly originating from vibrations of the flume. The forcing of the pumps gives narrow peaks. Waves probably influence the frequency range under 3 Hz. Noise is mainly caused by vibration, and less by acoustic waves.

### Filtering

Large vibrational noise can be removed by subtracting the signals from two pressure transducers placed at some distance from each other, although that allows only spectral features to be measured. The time history can be slightly improved by filtering with the 'optimal' filter.

### Requirements for future measurements

A new experimental facility should be influenced less by external vibrations. Vibrations of the floor itself need to be damped and the natural frequencies of the structure must be either very high ($> 300$ Hz) or very low ($< 5$ Hz). The in- and outflow must not cause any acoustical vibrations in the frequency range of interest. When the reference pressure is kept at a level near the hydrostatic pressure at the position of the pressure sensor, pressure sensors with a smaller range can be used, so that the background noise caused by the instrumentation will be lower, relative to the measured signal.

# References


ARMENIO, R., TOSCANO, P., & FIOROTTO, V. 2000. On the effect of a negative step in pressure fluctuations at the bottom of a hydraulic jump. *Journal of Hydraulic Research*, **38**(5).

BENDAT, J.S., & PIERSOL, A.G. 1971. *Random Data: analysis and measurement procedures.* Wiley-Interscience.

BENDAT, J.S., & PIERSOL, A.G. 1980. *Engineering applications of correlation and spectral analysis.* Wiley-Interscience.

BLAKE, W.K. 1970. Turbulent boundary-layer wall-pressure fluctuations on smooth and rough walls. *Journal of Fluid Mechanics*, **44**(4), 637–660.

BLAKE, W.K. 1986. *Mechanics of flow induced sound and vibration.*

BOOIJ, R. 1998. *Erosion under a geometrically open filter.* Tech. rept. 2-98. Delft University of Technology. In Dutch.

CHANG, P.A., PIOMELLI, U., & BLAKE, W.K. 1999. Relationship between wall-pressures and velocity-field sources. *Physics of Fluids A*, **11**(11), 3434–3448.

DE GUNST, M. 1999. *Stone stability in a turbulent flow behind a step.* M.Sc. thesis, Delft University of Technology, Delft. In Dutch.

FARABEE, T.M., & CASARELLA, M.J. 1991. Spectral featurs of wall pressure fluctuations beneath turbulent boundary layers. *Physics of Fluids A*, **3**(10), 2410–2420.

GRAVANTE, S.P., NAGUIB, A.M., WARK, C.E., & NAGIB, H.M. 1998. Characterization of the pressure fluctuations under a fully developed turbulent boundary layer. *AIAA Journal*, **36**(10).

HOFLAND, B. 2000. *Stability of stones in the top layer of a granular filter – literature survey.* Tech. rept. 07-00. Delft University of Technology.

LAUCHLE, G.C., & KARGUS IV, W.A. 1999. Scaling of turbulent wall pressure fluctuations downstream of a rearward facing step. *Acoustics research letters online.*

LÖFDAHL, L., GLAVMO, M., & JOHANSSON, B. 1993. A Silicon Transducer for the determination of Wall-Pressure Fluctuations in Turbulent Boundary Layers. *Applied Scientific Research*, **51**, 203–207.

NAGUIB, A.M., GRAVANTE, S.P., & WARK, C.E. 1996. Extraction of turbulent wall-pressure time-series using an optimal filtering scheme. *Experiments in Fluids*, **22**, 14–22.

SCHEWE, G. 1983. On the structure and resolution of wall-pressure fluctuations associated with turbulent boundary-layer flow. *Journal of Fluid Mechanics*, **134**, 311–328.

UITTENBOGAARD, R., HOFFMANS, G., & AKKERMAN, G.J. 1998. *Turbulence schematization for stone stability assessment.* Tech. rept. Q2395.30. WL|Delft Hydraulics, Delft.

XINGKUI, W., & FONTIJN, H.L. 1993. Experimental study of the hydrodynamic forces on a bed element in an open channel with a backward-facing step. *Journal of Fluids and Structures*, **7**, 299–318.

# Appendix A

# Companies contacted

**Orienterend onderzoek naar beschikbaarheid van drukmeters**

| Fabrikant | vraag | antwoord | Type no. | Soort + opmerkingen | Frequentie (Hz) liefst 400, min 100 | Bereik (mBar) ca. 5 | Nauwkeurigheid (0.01mBar) liefst 0.01, min 0.05 | Oordeel | Kosten (fl) |
|---|---|---|---|---|---|---|---|---|---|
| Omega | 17-4 | 18-4 | | Hebben het niet | | | | nee | |
| Kulite | 17-4 | 18-4 | | Hebben het niet | | 350 | ca. 0.9 | nee | |
| Intersema | 17-4 | 18-4 | (MS761-D) | Hebben het niet, wel goede hints | | 1000 | 1.5 | nee | |
| Feteris | 17-4 | 1-5 | | Hebben het niet | | | | nee | |
| Xensor integrations | 1-5 | 1-5 | | Tailor made: duur: is aanwezig op markt | | | | nee | |
| Druck nl | 17-4 | 1-5 | ja | piezo-resistief | ? | 75 | 0.04 | ja (?) | ca.4500,- |
| Scanivalve | 17-4 | 25-4 | | Hebben het niet | | 25 | | nee | |
| Sensortechnics | 17-4 | 26-4 | lpx/lpm5000ser | is type van Druck en is groot | 100 (?) | 0.5-50 | 0.01%(0.005) | nee | |
| TRW-Novasensor | 1-5 | 3-5 | NPC1210LP | piezo-resistief | ? | 25 | 0.12 | misschien | |
| Motorola | 1-5 | 11-5 | | piezo-resistief silicium chip | | 40 | 1 | nee | |
| Sensym | 1-5 | - | | | | | | ? | |
| Entran | 17-4 | - | | | | | | ? | |
| Honeywell | 17-4 | 8-5 | 24PCEFA6G | piezo-resistief silicium-chip | | 34.5 | ca. 0.14 | misschien | ca.45,- |
| Analog | 17-4 | 3-5 | | piezo-resistief silicium-chip | | 10 of 20 | | misschien | |
| Kistler | 17-4 | - | | we hebben folders van Geveke | | | | nee | |
| Geveke | 17-4 | 3-5 | van Kistler | | | 200 | | nee | |

# Appendix B

# Technical specifications of *Druck* sensor

# **MINIATURE SERIES:** High Performance Transducers

## INTRODUCTION

**Druck's experience with silicon diaphragm micro machining technology is considerable.**

For more than 15 years a commitment to continuous research and development in this field using the very latest techniques and equipment has culminated in some remarkable achievements in pressure transducer design and performance.

The miniature series is a typical example of the benefits of such work. A range of high accuracy sensors complete with thermal compensation in a miniature package providing maximum performance with minimal size and weight.

The silicon diaphragm is intricately micro machined, and semi-conductor strain gauges are diffused into the substrate to become an atomic part of the diaphragm. Each gauge is connected to form a wheatstone bridge configuration, which is subsequently terminated to offset and thermal compensation circuitry.

High signal outputs, excellent linearity, negligible hysteresis and good repeatability performance with considerable improvements in long term stability are the benefits of using Druck miniature pressure transducers.

**Your Specific Requirements**
In addition to the sensors shown, Druck have the engineering capability to design pressure transducers to specific individual requirements. By careful consideration of the configuration, environments, compatibility and other important performance characteristics, our engineering team can design, build and exhaustively test instruments for your needs.

Please contact our Sales Office for further information.

| GENERAL PURPOSE | | SCANIVALVE | PORE WATER |
|---|---|---|---|
|  Scale: 2:1 |  | 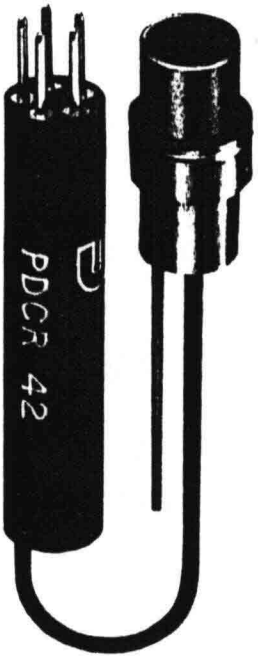 |  |
| PDCR 200 | PDCR 35 | PDCR 42 | PDCR 81 |

PDCR 200 Pressure units and range identification

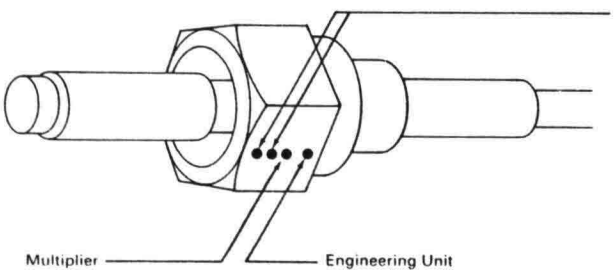


## ORDERING INFORMATION

Please state the following:-
(1) Type number
(2) Pressure range
(3) Gauge or differential
(4) Temperature range
(5) Pressure connection
(6) Pressure media

*For non-standard requirements please specify in detail.*

*Continuing development sometimes necessitates specification changes without notice.*

# **MINIATURE SERIES:** Specification

| | GENERAL PURPOSE | | SCANIVALVE | PORE WATER |
|---|---|---|---|---|
| **TYPE** | **PDCR 200** | **PDCR 35** | **PDCR 42** | **PDCR 81** |
| FEATURES | FLUSH MOUNTING<br>CHOICE OF MOUNTING THREADS<br>HIGH OUTPUT | RUGGED CONSTRUCTION | HIGH ACCURACY<br>HIGH OVERLOAD CAPABILITY | CERAMIC FILTER<br>RUGGED CONSTRUCTION<br>LONG TERM SURVIVABILITY |
| **Standard Specification** Operating pressure ranges **(1)** | 1, 2, 3, 6, 15, 30 and 60 bar gauge or differential **(2)** | 700 mbar, 1, 1.5, 2, 3.5, 5, 7, 10, 15, 20 and 35 bar gauge **(2)** | 75 mbar, 175 mbar, 350 mbar, 700 mbar, 1, 3, 5, 7, 14, 20 and 35 bar gauge or differential **(2)** | 75 mbar, 350 mbar, 1, 3, 7, 15 and 35 bar gauge |
| Overpressure (with negligible effect on calibration) | 3 x for all ranges **(3)**<br>(2 x for 1 and 2 bar range on reference side) | 4 x for all ranges **(3)** | 10 x for 75 and 175 mbar range **(3)**<br>6 x for 350 mbar range<br>4 x for 700 mbar range and above | 20 x for 75 mbar range<br>10 x for 350 mbar range<br>5 x for 1 bar range<br>3 x for 3 bar range and above |
| Positive pressure media | Fluids compatible with silicon, titanium and epoxy adhesive (and ceramic porous plate for PDCR 81) | | | |
| Reference pressure media | Dry, non-conducting gases | | | |
| Transduction principle | Integrated silicon strain gauge bridge | | | |
| Excitation voltage | 10 Volts 6mA nominal | 10 Volts 5mA nominal | 12 Volts 8mA nominal | 5 Volts 6mA nominal (10 volts max.) |
| Output voltage (nominal) at stated excitation | 150 mV for all ranges | 100 mV for all ranges | 15 mV for 75 mbar range,<br>25 mV for 175 mbar range,<br>50 mV for 350 mbar and 700 mbar range,<br>75 mV for 1 bar range and above | 15 mV for 75 mbar range,<br>35 mV for 350 mbar range,<br>50 mV for 1 bar range,<br>75 mV for 3 bar range and above |
| Zero offset **(4)** | ±15 mV maximum | ±5 mV maximum | ±3 mV maximum | ±10 mV maximum |
| Span setting | ±30% of nominal output | ±3 mV maximium **(4)** | | ±20% of nominal output |
| Output impedence (nominal) | 1500 ohms | 2000 ohms | 1000 ohms | |
| Load impedence | Greater than 100 kohms for quoted performance | | | |
| Resolution | Infinite | | | |
| Combined non-linearity and hysteresis | ±0.3% B.S.L. | ±0.1% B.S.L. | ±0.06% B.S.L. **(5)** | ±0.2% B.S.L. |
| Operating temperature range | -20° to +120°C **(6)** | -20° to +80°C **(6)** | -40° to +80°C **(6)** | -20° to +120°C **(6)** |
| Temperature effects | ±1.5% total error band<br>10° to 60°C **(7)** | ±1.0% total error band<br>0° to 50°C **(7)** | Thermal zero shift<br>±0.02% F.S./°C<br>(75 mbar range ±0.05% F.S./°C)<br>Thermal sensitivity shift<br>±0.02% of reading/°C<br>10° to 40°C **(7)** | Thermal zero shift<br>±0.05% F.S./°C<br>Thermal sensitivity shift<br>±0.2% of reading/°C<br>**(7) (8)** |
| Natural frequency (mechanical) | 75 kHz for 1 bar range increasing to 580 kHz for 60 bar range | 56 kHz for 350 mbar range increasing to 360 kHz for 35 bar range | | |
| Acceleration sensitivity | 0.002% F.S./g for 1 bar decreasing to 0.0005% F.S./g for 60 bar range | 0.003% F.S./g for 350 mbar decreasing to 0.0002% F.S./g for 35 bar range | | 0.005% F.S./g for 350 mbar decreasing to 0.0003% F.S./g for 35 bar range |
| Mechanical shock | 1000g for 1ms in each of three mutually perpendicular axis will not effect calibration | | | |
| Weight (nominal) | 12 grams | 12 grams | 10 grams | 30 grams with 5 metres cable |
| Electrical connection | 1 metre shielded integral cable **(9)** | | 20 cm integral cable connects transducer and compensation package. Free socket supplied | 5 metres integral Teflon vented cable |

**Key to table above**

**(1)** Other pressure units can be specified, e.g. psi, kPa, etc.

**(2)** For absolute pressures a vacuum can be pumped on the reference side.

**(3)** The transducers can be used in a bi-directional differential mode up to ±1 bar.

**(4)** More accurate settings available.

**(5)** ±0.04% B.S.L. available.

**(6)** Temperature range can be extended.

**(7)** For special applications it is possible to give improved temperature effects over a wider temperature range.

**(8)** Constant current operation ±0.05% of reading/°C typical.

**(9)** Longer lengths available.

# Appendix C

# Technical specifications of *Honeywell* sensor

**Honeywell**

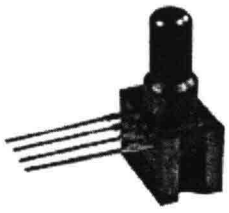

*Representative photograph, actual product appearance may vary.*

# 24PCEFA6D

**Pressure Sensors: Measurement Type: Differential; Signal Conditioning: Unamplified; Pressure Range: 0.5 psi; Port Style: Straight**

*Due to regional agency approval requirements, some products may not be available in your area. Please contact your regional Honeywell office regarding your product of choice.*

## Features

- Miniature package
- Variety of gage pressure port configurations - easily and quickly modified for your special needs
- Operable after exposure to frozen conditions
- Ideal for wet/wet differential applications
- Choice of termination for gage sensors
- 2 mA constant current excitation significantly reduces sensitivity shift over temperature*
- Can be used to measure vacuum or positive pressure

*Non-compensated pressure sensors, excited by constant current instead of voltage, exhibit temperature compensation of Span.Constant current excitation has an additional benefit of temperature measurement. When driven by a constant current source, a silicon pressure sensor's terminal voltage will rise with increased temperature. The rise in voltage not only compensates the Span, but is also an indication of die temperature.

# 24PCEFA6D

**Pressure Sensors: Measurement Type: Differential; Signal Conditioning: Unamplified; Pressure Range: 0.5 psi; Port Style: Straight**

| Product Specifications | |
|---|---|
| **Measurement Type** | Differential |
| **Signal Conditioning** | Unamplified |
| **Pressure Range** | 0.5 psi |
| **Maximum Overpressure** | 20 psi |
| **Temperature Compensation** | No |
| **Output Calibration** | No |
| **Output Type** | mV |
| **Supply Voltage** | 10 Vdc typ., 12 Vdc max. |
| **Sensitivity** | 70 mV/psi typ. |
| **Response Time** | 1 ms max. |
| **Termination** | PCB; 1 x 4; 0.600 in |
| **Port Style** | Straight |
| **Package Style** | Honeywell - 20PC |
| **Full Scale Span** | 24 mV min., 35 mV typ., 46 mV max. |
| **Linearity** | ± 0.25 % span typ., ± 1.0 % span max. (P2>P1) |
| **Null Offset** | -30 mV min., 0 mV typ., 30 mV max. |
| **Null Shift over Temperature** | ± 2.0 mV typ. |
| **Span Shift Over Temperature** | ± 5.0 % span typ. |
| **Repeatability & Hysteresis Error** | ± 0.15 % span typ. |
| **Operating Temperature Range** | -40 °C to 85 °C [-40 °F to 185 °F] |
| **Storage Temperature Range** | -55 °C to 100 °C [-67 °F to 212 °F] |

| | |
|---|---|
| **Media Compatibility** | Limited only to those media which will not attack polyetherimide, silicon, fluorosilicone, silicone, EPDM, and neoprene seals. |
| **Input Resistance** | 5.5 Kohms min., 7.5 Kohms typ., 11.5 Kohms max. |
| **Output Resistance** | 1.5 Kohms min., 2.5 Kohms typ., 3.0 Kohms max. |
| **Shock** | Qualification tested to 150 g |
| **Vibration** | MIL-STD-202 Method 213 (150 g half sine 11 ms) |
| **Weight** | 2 g [0.07 oz] |
| **UNSPSC Code** | 411121 |
| **UNSPSC Commodity** | 411121 Transducers |
| **Availability** | Global |
| **Series Name** | 24PC Series |

# 24PCEFA6D

**Pressure Sensors: Measurement Type: Differential; Signal Conditioning: Unamplified; Pressure Range: 0.5 psi; Port Style: Straight**

**Straight Port, 1 x 4 Termination (Style 1) ONLY**

Port 1 is near terminals

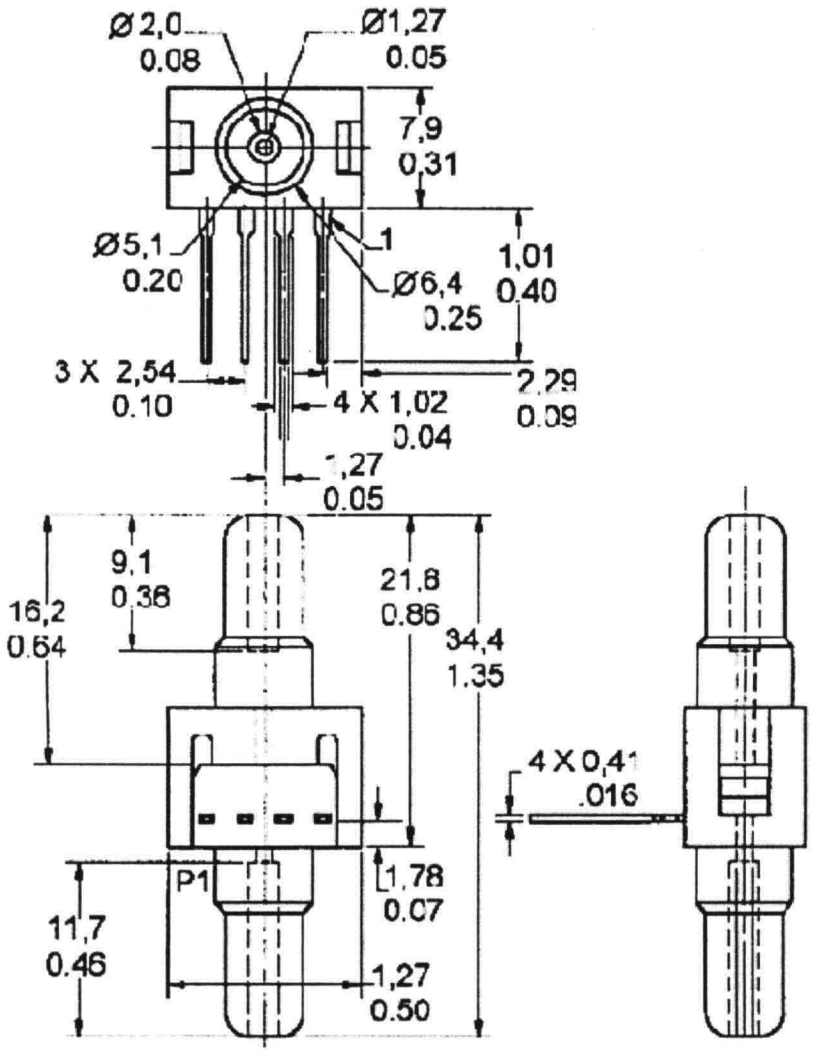

# Appendix D

# Definitions of spectral functions

The definitions for various spectral functions are given in this appendix:
The finite-range Fourier transform of signal $x$ with duration $T$ is defined as:

$$X(f) = \int_0^T x(t)e^{-i2\pi ft}dt \tag{D.1}$$

With its discrete version:

$$X(f,T) = \Delta t \sum_{m=0}^{N-1} x(m)e^{-i2\pi \frac{km}{N}} \tag{D.2}$$

where $\Delta t$ is the sample distance.
The auto (variance density) spectrum is defined as:

$$G_{xx}(f) = \lim_{T\to\infty} \frac{2}{T} X(f,T)X^*(f,T) \tag{D.3}$$

The finite-range and discrete approximation of $G_{xx}$ is:

$$G_{xx}(f) \approx \frac{2}{T} X(f,T)X^*(f,T) \tag{D.4}$$

The cross spectrum of signals $x$ and $y$, with fourier transform $X(f,T)$ and $Y(f,T)$ is defined as:

$$G_{xy}(f) \approx \frac{2}{T} X^*(f,T)Y(f,T) \tag{D.5}$$

The coherence function is defined as:

$$\gamma_{xy}^2 = \frac{|G_{xy}(f)|^2}{G_{xx}(f)G_{yy}(f)} \tag{D.6}$$

The transfer function (frequency response function) is defined as:

$$H_{xy} = \frac{G_{xy}(f)}{G_{xx}(f)} \tag{D.7}$$

$|H_{xy}|$ is defined as the gain factor, and the phase angle is:

$$\theta(f) = \arctan \frac{\operatorname{Im} G_{xy}(f)}{\operatorname{Re} G_{xy}(f)} \tag{D.8}$$

A variance preserving or premultiplied spectrum of $G_{xx}$ is plotted as: ${}^{10}\log(x)$ against $f \cdot G_{xx}$. The area under this graph still represents the variance of the signal although the horizontal axis is logarithmic.